NUREG/CR-3639
SAND84-0040

Large Break LOCA Analyses for Two-Loop PWRs with Upper-Plenum Injection

Prepared by D. Dobranich, L. D. Buxton

Sandia National Laboratories

Prepared for
U.S. Nuclear Regulatory Commission

GPO Printed copy price: $4.50

NUREG/CR-3639
SAND84-0040

Large Break LOCA Analyses for Two-Loop PWRS with Upper-Plenum Injection

Manuscript Completed: February 1984
Date Published: May 1984

Prepared by
D. Dobranich*, L. D. Buxton

Sandia National Laboratories
Albuquerque, NM 87185

Prepared for
Division of Systems Integration
Office of Nuclear Reactor Regulation
U.S. Nuclear Regulatory Commission
Washington, D.C. 20555
NRC FIN A1294

*Science Applications, Inc.
Albuquerque, NM 87102

ABSTRACT

A series of best-estimate thermal-hydraulic calculations was performed using TRAC-PF1 to simulate a hypothetical loss-of-coolant accident in Westinghouse two-loop pressurized water reactors. Those reactors are equipped for low-pressure injection of emergency coolant directly into the upper plenum of the reactor vessel. This type of injection is referred to as upper plenum injection (UPI). The calculations were performed to evaluate the effectiveness of UPI compared to injection into the vessel downcomer, referred to as downcomer injection (DI).

The TRAC results indicated that some channeling of upper plenum injected liquid down the core periphery occurred; however, a large percentage of that liquid was vaporized as it drained toward the lower plenum. This vaporization degraded the bottom-flood quench front compared to that seen in TRAC calculations in which downcomer injection was assumed. For the case of upper plenum injection, counter-current flow limiting conditions at the upper core support plate led to formation of a large subcooled liquid pool in the upper plenum; part of this subcooled liquid was entrained into the hot legs and steam generators. Only a small saturated liquid pool formed in the case of downcomer injection. Overall, the calculations show that higher peak clad temperatures are produced when the low-pressure injection is into the upper plenum instead of the vessel downcomer.

CONTENTS

LIST OF FIGURES

LIST OF TABLES

GLOSSARY

CCFL	Counter-Current Flow Limiting
D	Diameter
DI	Downcomer Injection
ECC	Emergency Core Cooling
EM	Evaluation Model
FSAR	Final Safety Analysis Report
FW	Feedwater
GT	Guide Tube
HPI	High-Pressure Injection
L	Length
LOCA	Loss-Of-Coolant Accident
LPI	Low-Pressure Injection
NRC	Nuclear Regulatory Commission
PCT	Peak Clad Temperature
PWR	Pressurized Water Reactor
SC	Support Column
SG	Steam Generator
UCSP	Upper Core Support Plate
UPI	Upper Plenum Injection
1-D	One Dimensional
3-D	Three Dimensional
f	friction coefficient

ACKNOWLEDGMENTS

The authors wish to acknowledge Lubomyra N. Kmetyk along with C. Channy Wong for their efforts involving the collection and cataloging of the plant data necessary for the preparation of the computer input decks. C. Channy Wong also contributed to this work through many discussions with the authors involving numerous technical aspects of the results. Special thanks go to Katherine McFadden for her graphics and computer-related assistance and to Jan Frey for her preparation of the final report.

EXECUTIVE SUMMARY

Best-estimate thermal-hydraulic calculations were performed to investigate a loss-of-coolant accident in Westinghouse two-loop pressurized water reactors (PWRs) equipped with upper plenum injection (UPI). The term UPI refers to low-pressure injection (LPI) of emergency coolant into the upper plenum of the reactor vessel. The thermal-hydraulic calculations were performed using TRAC-PF1. An integral model was developed for TRAC using a simple noding scheme for the vessel. A second model, the detailed model, was developed which used a more elaborate noding scheme for the vessel. The detailed model, however, used a much simpler loop noding scheme compared to the integral model. The integral model was used to simulate the entire transient. Results from the integral-model calculations also provided initial conditions for the detailed model, which was used to simulate only the reflood phase of the transient.

Using the integral model, two cases were considered: case UPI -- with LPI liquid injected into the upper plenum as designed; and case DI -- with LPI liquid injected into the downcomer, similar to the modeling used for current licensing calculations.

The peak clad temperature (PCT) for case UPI occurred at a higher value and at a later time than for case DI; 1030 K at 160 s for case UPI compared to 940 K at 75 s for case DI. The PCT for a hot rod with a hot-to-average power ratio of 1.2 was 1100 K for UPI versus 1000 K for DI.

The core midplane elevation did not quench for case UPI until 330 s, while the midplane elevation was quenched at 180 s for case DI. One reason for the differing reflood response in these two calculations is that case UPI had a large falling-film quench front at the expense of a slower moving bottom-flood quench front. The slower moving bottom quench front, therefore, took longer to reach the core midplane, the region of highest power. Another way to view this is that the LPI liquid in case DI contributed directly to the bottom flood whereas case UPI had more nearly equal bottom-flood and falling-film quench fronts propagating toward the midplane at slower rates than the bottom flood alone of case DI.

A second reason for the differing reflood response is that, for case UPI, the injected liquid formed a large pool on the upper core support plate. Some of this liquid was entrained into the hot legs by vapor generated in the vessel. There the liquid

was heated by contact with the hot-leg walls. Some of this trained liquid reached the steam generators, which acted as heat sources, and was vaporized. The resulting pressure increase reversed the hot-leg flow (now consisting mostly of saturated vapor) back into the upper plenum. The net result of this oscillatory flow was that a significant amount of the cooling capacity of the injected liquid was used outside the reactor vessel. In fact, for case UPI, the hot legs added an average of 8 MW of power during reflood to the injected liquid before it had a chance to enter the core. For case DI, the hot legs added only 3 MW to the liquid and this was after the liquid had already provided core cooling. Therefore, UPI resulted in less effective use of the injected liquid.

Calculations for the same two cases were performed using the detailed model; case UPI' and case DI'. Comparing case DI and case DI', the results were generally the same because 3-D effects in the core did not have a substantial influence on the progression of the transient when liquid was injected into the downcomer. The PCT was reached at about the same time (70 s) for both cases at a value of 960 K for case DI' compared to 940 K for case DI. The loop response for both cases was almost identical.

Comparing case UPI and case UPI', the results were also quite similar. However, 3-D effects in the core and upper plenum did prove to be significant with respect to PCT. Partial channeling of the injected liquid down the outer regions of the core in case UPI' reduced the amount of interaction with the core and resulted in a higher bottom-flood quench rate. The PCT reached for case UPI' was 1000 K compared to 1030 K for case UPI.

The results of both the integral-model and the detailed-model calculations showed an increase in PCT when LPI liquid was injected into the upper plenum compared to when LPI liquid was injected into the downcomer. The detailed-model calculations showed less increase because that model included the effects of channeling in the reactor core.

1.0 INTRODUCTION

1.1 Background and Statement of Problem

There are six operating two-loop plants in the United States with upper-plenum injection (UPI). The reason for UPI on two-loop plants is so that no single failure associated with a cold-leg break can defeat the emergency core cooling (ECC) system. The thermal-hydraulic evaluation model (EM) originally approved by the Nuclear Regulatory Commission (NRC) for two-loop plants includes the assumption that the low-pressure injection (LPI) liquid is delivered to the lower plenum via the cold legs rather than through the core from the upper plenum. This simplified treatment of UPI allowed the use of the same evaluation model for two-, three-, and four-loop plants.

There is a current concern in the NRC that the existing EM calculations for two-loop plants do not conservatively account for the effects of injecting LPI liquid into the upper plenum. The effects may include: (1) increased steam generation in the core that would retard the bottom reflood, (2) increased entrainment of injected liquid at the upper core support plate (UCSP), and (3) increased condensation in the upper plenum.

The objective of this analysis is to investigate the aforementioned effects with respect to the prediction of the peak clad temperature (PCT) during a large-break loss-of-coolant accident (LOCA). This investigation will help in determining the effectiveness of upper plenum injection with respect to cold leg or downcomer injection of LPI liquid.

1.2 Approach to Problem

The Transient Reactor Analysis Code, TRAC-PF1 (9.2), [1] was chosen as the principal computational tool because of its best-estimate thermal-hydraulic capability along with its provision for modeling the vessel in three dimensions. Previous versions of TRAC (P1A, PD2, PD2/MOD1) have been assessed against data from a broad range of experimental facilities. Version PF1 has not yet undergone such an assessment, but represents the most sophisticated version available. Besides offering more versatility, version PF1 attempts to correct many of the identified deficiencies and errors of the previous versions.

Detailed three-dimensional (3-D) calculations for an entire LOCA simulation are time consuming and costly. Therefore, we tried to reduce costs by using a strategy whereby two different TRAC models can be employed in sequence -- an integral model and a detailed model. (See Appendix A for calculation timing statistics.)

The integral model contains the entire primary system including a one-dimensional (1-D) treatment of all ex-vessel components and a simple three-dimensional treatment of the vessel. This model is used to simulate an entire LOCA (starting from code-generated steady-state conditions) including blowdown, refill, and reflood.

The detailed model includes a finely-noded three-dimensional representation of the vessel. The ex-vessel components are modeled with one-dimensional pipes to represent the steam generators and loops. This ex-vessel model is much simpler than that of the integral model.

The results of the integral model are then used to provide boundary conditions to the detailed model starting at the end of the refill phase of the accident. In this way, the interaction of the LPI liquid in the vicinity of the UCSP can be investigated in detail. This approach saves a significant amount of computer time while retaining the accuracy required to resolve the dynamic effects expected to occur in the vessel. Parametric cases can also be easily run with this approach.

Both TRAC models (integral and detailed) are used to simulate a LOCA with two different methods of injecting LPI liquid into the vessel. The first method assumes injection into the upper plenum as designed while the second method assumes injection into pipes connected to the downcomer close to the cold-leg nozzles. The second method, downcomer injection, was chosen because it closely approximates the current EM assumption that LPI liquid is delivered directly to the lower plenum via the cold legs. Also, the possibility of flow around the downcomer and out the break (bypass) is accounted for in the TRAC model. Comparison of results can easily be made for the two different methods of injection because the calculations are performed with essentially the same input model and the same computer code.

2.C INTEGRAL MODEL

2.1 Integral Model Description and Steady State Results

A generic two-loop plant was modeled for the analysis. Information for this model was obtained from proprietary Westinghouse drawings and documents supplied by the NRC and from publicly available final safety analysis reports (FSARs) for various two-loop plants. Also, some additional information was obtained by direct contact with Westinghouse personnel. The input deck was designed to simulate large-break LOCAs using best-estimate operating assumptions and initial conditions.

The ex-vessel components modeled include the hot- and cold-leg piping, pressurizer, main coolant pumps, steam generators (SG) with main feedwater (FW) injection, high- and low-pressure injection (HPI and LPI), accumulator check valves, and accumulators. A total of 113 one-dimensional mesh cells was used to model these components and an additional 16 cells were used to model the support columns (SCs) and guide tubes (GTs) in the vessel upper plenum. A schematic of the model is shown in Figure 1, and Table I contains a breakdown of the noding by component. Except for the pressurizer and surge line, all components are identical for both loops of the plant. The accumulators and HPI were modeled on both loops. Form loss coefficients (friction) were added to the accumulator lines based on Westinghouse-supplied fL/D data. Injection of accumulator nitrogen into the primary was not modeled because TRAC's ability to predict its effects on large-break LOCAs has not been assessed.

The downcomers on the steam generator secondaries were not modeled separately. However, the liquid volume of the SG downcomers was added to the SG secondary inventory. The fluid temperature that would occur at the bottom of the SG downcomer, assuming a representative recirculation ratio, was input for the FW temperature instead of using the actual FW temperature. The FW flow was then adjusted accordingly. This provided the correct amount of primary-to-secondary energy removal along with the correct amount of heat capacity on the secondary side.

The vapor-liquid separation in the SG was modeled by using artificially-large flow areas at the top of the SG secondary. This lowered the interfacial drag and prevented liquid entrainment by the exiting vapor. Because the SG secondary-side downcomer was not modeled separately, this modification was necessary to accurately predict the secondary-side liquid inventory.

Table I: Integral Model Noding for One-Dimensional Components

Component	Component #	# of Cells
Hot Legs:	30, 40	10
Steam Generators:	31, 41	
Primary		24
Secondary		16
Feedwater Inlets:	11, 13	2
Feedwater Exits:	12, 14	2
Loop Seals:	32, 42	8
Pumps:	33, 43	4
Cold Legs:	24, 44	8
LPI Lines:	81, 91	4
LPI:	80, 90	2
ECC Injection Tees:	61, 71	6
HPI:	62, 72	2
Accumulator Check Valves:	60, 70	8
Accumulators:	63, 73	8
Pressurizer Surge Line:	30	3
Pressurizer:	50	5
Pressurizer Top:	51	1
Support Columns:	23, 24	8
Guide Tubes:	21, 22	8
Total (both loops):		129

The vessel was modeled using the three-dimensional capability of TRAC with two radial segments, two azimuthal sectors, and 13 axial levels. A noding diagram for the vessel is given in Figure 2. Consideration was given to using all 1-D components for the vessel, but this possibility was rejected because of the complexity of joining the 1-D components to accurately represent the geometry of the vessel.

The two hot legs and two cold legs were connected to level ten and the LPI lines connected to level nine. The plant LPI lines actually connect at the same elevation as the hot legs, but because of source limitations in TRAC (only 1 source connection per cell) and because only two azimuthal sectors were used in the vessel model, they were connected one level below. The additional gravitational pressure head associated with this elevation difference of 0.8 m would be less than 0.1 bars (0.1×10^5 Pa) and is not expected to significantly change the delivery rate of the LPI.

In general, the axial levels were chosen to coincide with the location of support plates. In the case where several plates were located close together (e.g. tie plate and diffuser plate), the flow area fraction corresponding to the most restrictive plate was used. The support columns and guide tubes were modeled with one-dimensional pipes connecting the core to the upper head (the SC and GT metal mass was included with the vessel upper plenum metal mass). The UCSP contains a total of 121 round and square holes. Thirty-seven of these holes are covered by square GTs and thirty-one are covered by round SCs. In the calculation of the UCSP axial flow area, it was assumed that holes covered by the GTs and SCs were completely blocked. The total flow area for the UCSP is 1.2614 m^2 (or a flow area fraction of .1967). The total flow area for the core is 2.5028 m^2 (flow area fraction of .3903).

The barrel-baffle region was not modeled separately; however, its volume was included in the core. The flow blockage of the thermal shield was accounted for in the downcomer flow area fraction and its mass was included in the vessel walls. Flow areas at the top of the downcomer were included to model the cooling jets. Large flow areas and associated friction values were applied to the cooling jets to prevent Courant time-step limitations during the transient without affecting the predicted steady-state flow. To do this, TRAC was modified to allow user input of a vertical flow area at the top of the downcomer.

A distributed-slab conduction model with three nodes was used for the vessel heat slabs (structure) and radial conduction in the fuel rods was modeled using eight radial nodes (five in the fuel, one in the gap, and three in the clad). The fine-mesh option in TRAC was used, which allows a variable spacing between axial conduction nodes in the fuel. A minimum of 30 and a maximum of 100 axial nodes are used. The nodes are inserted or removed during reflood depending on the magnitude of the axial temperature gradients. The relative axial-power factors used for the five core-level interfaces were: 0.2065, 0.7391, 1.0, 0.7391, 0.2065. The average and peak linear-power-generation rates per rod were 5.85 kw/ft and 8.72 kw/ft, respectively. TRAC also allows the user to specify a hot-rod peaking factor. This factor is multiplied by the average-rod power to define a hot rod. Although the hot rod does not interact with the fluid hydraulics, a conduction calculation is performed for this rod using the average-rod fluid conditions. Such a hot rod was defined using a peaking factor (hot-to-average power ratio) of 1.2.

The generalized steady-state option in TRAC was used to calculate the thermal-hydraulic fluid properties during normal plant operation. User-specified friction was added where necessary to achieve the desired pressure drops and flows throughout the loops. This was done without ensuring that the amount of

friction used was geometrically justified by accepted resistance coefficients for area changes and bends. Also, friction was added to the SCs and GTs to provide the flow necessary to achieve the desired upper head fluid temperature. The desired and calculated steady-state conditions are shown in Table II. The desired conditions predominantly represent FSAR information. They do not come from any single two-loop plant, but instead represent generic data.

Table II: Steady-State Conditions

Parameter	Desired	TRAC
Core power, MWt	1520	1520*
Total loop flow, kg/s	8497	8474
Cooling-jet flow, kg/s	22.9	23.7
Core inlet temperature, K	562.2	560.8
Vessel-head liquid temperature, K	583	584
System pressure, MPa	15.51	15.51*
Pump ΔP, kPa	580	582
Lower support and diffuser plate ΔP, kPa	11.2	14.3
Lower core plate ΔP, kPa	7.0	7.3
Core ΔP, kPa	128.4	128.5
Upper core plate ΔP, kPa	16.3	15.0
Steam generator secondary exit temperature, K	544.8	544.6
Steam generator secondary exit pressure, MPa	56.6	56.6*
Accumulator liquid volume (total), m^3	65.1	65.1*
Accumulator liquid temperature, K	325	325*
HPI/LPI liquid temperature, K	315	315*

* These parameters were specified by input

2.2 Integral Model Transient Results

2.2.1 Calculation Assumptions

A 200% double-ended rupture of the loop B cold leg (2.85 m from the vessel) was the initiating event. The rupture was modeled in TRAC by replacing the loop B cold-leg pipe with two separate pipes, each connected to a break component to simulate the containment.

Some of the operating assumptions for the calculation are summarized in Table III. Additionally, (1) the main coolant pumps remained running at constant speed during the transient, (2) both the HPI and LPI were input using tables of mass flow versus primary pressure (based on generic data for two-loop plants), (3) the containment pressure applied at the breaks was given in time-dependent tables (data taken from the Prairie Island FSAR and shown in Figure 3), and (4) the reactor decay power (Figure 4) was input for the calculations via tables based on standard ANS decay curves.

Table III: Operating Assumptions

Event	Signal	Comment
200% Cold-leg break, Isolate secondary	Time = 0.0	Initiating event
Reactor scram and FW Trip	Primary pressure less than 13.0 MPa plus 0.1 s delay	Power = 1520 MWt, FW coastdown in 30 s
HPI initiation	Primary pressure less than 11.98 MPa plus 1.0 s delay	Flow vs. pressure
Accumulator initiation	Primary pressure less than 4.95 MPa	Static check valve
LPI initiation	Primary pressure less than 1.25 MPa plus 2.0 s delay	Flow vs. pressure

Two cases were performed using the integral model. Case UPI assumes LPI into the upper plenum and case DI assumes the LPI enters the downcomer.

2.2.2 Case UPI Results

The timing sequence for this transient is summarized in Table IV. The core average pressure, given in Figure 5, shows that blowdown was over at approximately 18 s. The pump-side and vessel-side break flows are shown in Figures 6 and 7, respectively. The erratic behavior of the pump-side break flow from 13 to 27 s is a result of the way TRAC break components were used to model the containment. The subcooled accumulator liquid, entering the loop B piping just before the pump-side break, initially

condensed the vapor in the pipe adjacent to the break. The condensation lowered the pressure in the pipe below that of the containment and caused an inflow of saturated vapor from the containment. This incoming vapor then heated the leading surface of the subcooled liquid sufficiently to stop condensation and increase the pressure in the pipe, restoring flow out of the pipe to the containment. However, more subcooled liquid from the accumulator then entered the pipe and the process repeated. If air instead of saturated vapor had been specified in the containment, this oscillatory process would not have occurred. In either case, the loop B accumulator liquid would all go out the break. In fact, it is common practice in large-break LOCA analysis to not model the broken-loop accumulator at all because it has no significant influence on the transient.

The accumulator flow for loop A (the intact loop), shown in Figure 8, peaked at about 1700 kg/s and ended at approximately 28 s. At this time, the lower plenum was full and the core had a liquid volume fraction of about 0.1. The intact loop accumulator initially contained 35,000 kg of liquid. At the time the accumulator was empty, about 21,000 kg of liquid were contained in the downcomer and lower plenum. This indicates that about 14,000 kg (40%) of the initial accumulator inventory was bypassed to the break. The HPI and LPI flows are shown in Figures 9 and 10, respectively. All HPI and LPI pumps were assumed to operate during the LOCA.

Table IV: Case UPI Event Sequence

Event	Time(s)
200% Cold-leg break	0.0
Reactor scram and FW trip	.16
HPI initiation	1.1
Accumulator check valves open:	
Loop A	6.5
Loop B (broken loop)	3.0
LPI initiation	13.0
Pressurizer level less than 0.1 m	15.0
End of blowdown	18.0
Accumulator check valves close:	
Loop A	28.0
Loop B	25.0
Beginning of reflood	28.0
PCT reached (1030 K for average rod, 1100 K for hot rod)	160.0
Core midplane quench	330.0

A temporary decrease in the core liquid volume fraction (Fig. 11) occurred between 100 and 150 s. A partial voiding of the lower plenum at this time is also seen in the lower plenum liquid volume fraction shown in Figure 12. This voiding occurred when the liquid in the downcomer and lower plenum was heated to saturation resulting in a level swell.

The source of energy for this heating was the stored energy in the vessel structure and fuel rods along with the core decay power. With upper plenum injection, the LPI liquid was heated to saturation in the core before falling to the lower plenum. Therefore, the only subcooled liquid in the lower plenum and downcomer was the accumulator liquid (accumulator flow ended at 28 s) and the incoming intact-loop HPI liquid (some of which was being bypassed to the break along with some of the accumulator flow). Before 100 s, the energy was going into heating this subcooled liquid. Between approximately 100 and 150 s, the rate of energy going into the lower plenum and downcomer liquid exceeded the liquid's sensible cooling capacity and the liquid began to boil. After 150 s, the rate of energy input had decreased while the HPI and LPI continued to provide liquid at a constant rate. Boiling of liquid in the lower plenum and downcomer stopped and the level swell ended. The result of the level swell was the loss of a small amount of vessel inventory to the break. This caused a temporary delay in the progression of the bottom reflood, but had little effect on the remainder of the transient. The liquid in the upper part of the downcomer remained saturated, however, and continued to be vaporized and drawn out the break at a rate greater than if the liquid had remained subcooled.

Before the level swell period, small dips in the lower plenum liquid inventory occurred periodically with a relatively large dip at approximately 50 s. These dips occurred when slugs of liquid entered the core from either the lower or upper plenum. Vaporization of these slugs by the hot core increased the local pressure sufficiently to push some of the lower plenum liquid into the downcomer. The pressure increase at 50 s was large enough to push some of the lower plenum liquid out the break. After the level swell, the pressure increases were much smaller because most of the core had quenched by that time.

The LPI into the upper plenum slowly formed a liquid pool on the UCSP, as shown in Figure 13. The pool formed at a rate of about 15 kg/s. This pool (about 12 K subcooled on average) formed due to an intermittent counter-current flow limiting (CCFL), or flooding, condition in which the upward flow of vapor produced in the core was sufficient to prevent complete LPI liquid penetration into the core. With no further liquid penetration, however, vapor production decreased and some of the LPI liquid again penetrated into the core. This intermittent penetration is seen in Figures 14 and 15 which show the vapor and liquid mass flows, respectively, at the core exit.

Using Wallis' standard correlation for CCFL (see Appendix B), it was calculated that an upward vapor mass flow of 21 kg/s is necessary for complete flooding at the UCSP. This is consistent with the TRAC calculated response. The effects of radial power and geometric non-uniformity in the core and at the UCSP are considered in the detailed-model calculation in the next section.

Vapor generated in the core entrained some of the subcooled LPI liquid from the upper plenum into the hot legs where it was heated by the hot pipe walls. Some of the entrained liquid entered the steam generators, which served as heat sources, and was vaporized. Although the resulting pressure increase reversed the hot-leg flow back into the upper plenum, this backflow consisted mostly of saturated vapor which condensed on the LPI liquid pool. Hence, the occurrence of the pool formation was detrimental in that it led to a reduction in the cooling capacity of the LPI liquid available to the core. The mixture mass flow into the intact-loop hot leg is shown in Figure 16.

The rate of energy transfer to the fluid from the core, vessel structure, hot-leg walls, and SG secondaries is given in Table V. This table indicates that hot-leg cooling contributed 8.5% of the total energy released during the reflood phase of the transient. Another way to view this is to say that the power in the core was effectively increased by an average of 8 MW during reflood because of hot-leg cooling. During the initial part of blowdown, the SGs were heat sinks such that the net energy transfer from the SGs during the combined blowdown and refill period was negative. The SGs, therefore, are not included in the table for the blowdown and refill phase.

Table V: Energy Sources

	Avg rate of energy transfer to fluid during blowdown and refill (0-30 s)		Avg rate of energy transfer to fluid during reflood (30-335 s)	
Source	MW	% of Total	MW	% of Total
Core stored energy and decay power	370	80	72	76
Vessel structure stored energy	76	16	12	13
Hot-leg walls stored energy	17	4	8	8.5
SG secondary stored energy	*	*	2.5	2.6

Heat transfer in the hot-leg pipe walls was modeled using a lumped-parameter conduction algorithm. This was investigated further by also modeling the hot-leg wall heat transfer using a five-node radial conduction algorithm. Less energy transfer from the hot-leg walls to the liquid was predicted using this algorithm. However, more liquid flowed into the steam generators. For the 335 s of the transient, the steam generators essentially represented an infinite heat source that vaporized all the entering liquid. Therefore, the amount of hot vapor flowing back into the upper plenum was not strongly dependent on the number of radial nodes used in the pipe walls.

Both bottom-flood and falling-film quench fronts existed throughout the transient, propagating toward the core midplane. Figure 17 shows the maximum clad temperature of the average rods in the core. This figure was derived by plotting the maximum clad temperature found anywhere in the core as a function of time. The PCT was reached at about 160 s with a value of 1030 K and the core midplane quenched at approximately 330 s.

2.2.3 Comparison of Case UPI and Case DI

The sequence of events for case DI is the same as listed for case UPI (Table IV) except for the core quench times and the PCTs. Accumulator flow, HPI, LPI, power decay, and containment pressure were all the same for both cases. The blowdown and refill phases of the transient, therefore, were the same for both cases also. After around 30 s, however, the results began to diverge.

For case DI, only a small pool of liquid formed in the upper plenum. This pool formed as a result of entrained drops being carried up through the core and de-entraining on the UCSP. The average carry-over fraction (defined as the core-exit-liquid-flow rate divided by the core-inlet-liquid-flow rate) during reflood was 0.35.

Figure 18 shows the break flow for both cases starting at 200 s. For case UPI, the flow out the break during reflood was large (approximately 250 kg/s) because the low density (roughly 400 kg/m^3) two-phase mixture in the downcomer was easily carried out the break. (A positive pressure gradient from the downcomer to the break persisted because of the net production of vapor in the vessel.) For case DI, the LPI liquid entering the downcomer provided a source of subcooled liquid directly to the bottom of the core. The amount of subcooling in the lower plenum for both cases is shown in Figure 19. Although the liquid in the downcomer remained subcooled (high density), the increased driving potential (elevation head) of the liquid in the downcomer resulted in manometer oscillations between the core and downcomer. This resulted in large slugs of liquid being swept out the break. Figure 18 demonstrates this periodic slug break flow for case DI. The average flows out the breaks for both cases, however, were approximately equal.

Figure 20 shows that the core liquid volume fraction for case DI increased at about the same rate as for case UPI (see Figure 11). However, the available core cooling capacity was larger for case DI because very little LPI liquid was carried into the hot legs. The hot-leg wall temperature for both cases is shown in Figure 21, which illustrates the increased amount of hot-leg wall cooling for case UPI. In fact, an average of 8 MW of power was added during reflood to the LPI liquid from the hot legs for case UPI compared to only 3 MW for case DI. In case DI, however, the LPI liquid had already provided core cooling, whereas the LPI liquid for case UPI was swept into the hot legs before it had a chance to enter the core.

LPI cooling capacity can also be lost due to cooling of vessel structure. The vessel walls were cooled more for case DI while the upper plenum internals were cooled more for case UPI. The total amount of energy transferred from vessel structure to the fluid, shown for both cases in Figure 22, shows that case UPI contributed only slightly more energy (3%) than case DI. (Note that a minor mistake in defining the decay power curve for case DI resulted in a total of approximately 1.2% more decay energy input for that case over the entire 350 s of the transient. This mistake can be considered conservative for purposes of this analyses because its effect would be to increase the PCT for case DI, thereby decreasing the PCT difference between case DI and case UPI. It should be pointed out, however, that the PCT increase for case DI would be very small, probably less than 1 or 2 K.)

For case UPI, some of the LPI liquid was vaporized at the upper elevations of the core. This vaporization decreased the delivery rate of LPI liquid to the core, especially to the lower elevations of the core. The result was a degraded bottom-flood quench front compared to case DI. Figures 23 through 28 show the clad temperature at various axial locations. These figures demonstrate that, for case UPI, a large falling-film quench front existed. This, however, was at the expense of the bottom-flood quench front. The slower moving bottom-flood quench front, therefore, took longer to reach the core midplane, the region of highest power. Quench envelopes for both cases, shown in Figure 29, demonstrate the differing top and bottom quench rates.

Figure 30 shows the maximum average-rod clad temperature and Figure 31 shows the maximum hot-rod clad temperature for both cases. The PCT for case UPI occurred at a higher value and at a later time than for case DI; 1030 K at 160 s for case UPI and 940 K at 75 s for case DI. The PCT for the hot rod (with a hot-to-average power ratio of 1.2) was 1100 K for case UPI and 1000 K for case DI.

Three heat transfer regimes predominated in the core throughout reflood for both cases: nucleate boiling, transition boiling, and film boiling.

Nucleate boiling was the most effective heat transfer mechanism. The liquid heat transfer coefficient for this regime ranged from 1,500 to 10,000 watts/m^2/K with an average value during reflood of approximately 6,000. Film boiling was the least effective mechanism with an average liquid heat transfer coefficient of 10 watts/m^2/K and an average vapor heat transfer coefficient of 35 watts/m^2/K. Transition boiling may be considered a combination of nucleate boiling and film boiling with heat transfer coefficients ranging between the two. The average liquid heat transfer coefficient for transition boiling was 2,000 watts/m^2/K and the average vapor heat transfer coefficient was 50 watts/m^2/K. It should be kept in mind that reflood was highly turbulent and that heat transfer coefficients varied tremendously, depending on rapidly changing fluid conditions.

For case UPI, nucleate boiling occurred primarily at the bottom quench front as the liquid level in the core rose. Transition boiling occurred at the top of the core. Sometimes, however, nucleate boiling occurred as the LPI liquid penetrated the UCSP and entered the core. Film boiling occurred mostly in the center regions of the core in the presence of a highly dispersed liquid-vapor flow.

For case DI, again nucleate boiling occurred at the bottom quench front. Transition boiling extended above the bottom quench front due to liquid drops being entrained by the upward moving vapor. Film boiling occurred at the top of the core although there was some transition boiling when de-entrainment of liquid from the upper plenum occurred.

The heat transfer coefficients were larger at the top of the core for case UPI. As mentioned previously, however, this led to a decrease in the rate at which the nucleate boiling region at the lower elevations of the core advanced.

In summary, injection of LPI liquid into the upper plenum was less effective than injection into the downcomer with respect to PCT. This is because of horizontal entrainment of LPI liquid into the hot legs and SGs and because of a smaller delivery rate of LPI liquid to the bottom reflood.

3.0 DETAILED MODEL

3.1 Detailed Model Description

The detailed model includes the entire primary system. However, only the vessel was modeled in detail. Instead, the results from the integral model were used as a basis for optimizing the construction of the loops for the detailed model with a minimum number of mesh cells. This allowed a finer noding in the regions of most interest (the core and upper plenum) without imposing a penalty in the running time due to a large number of cells.

A total of only 31 one-dimensional mesh cells were used to represent the primary loops and steam generators. The SGs were modeled with pipe components. The flow area, wall area, and hydraulic diameter of the pipe were set equal to the flow area, wall area, and hydraulic diameter of the SG tubes. The mass of the pipe wall for the detailed model was adjusted to provide heat capacity equivalent to that of the combined tube walls and secondary-side fluid of the integral model. In this way, the secondary energy content and the rate of energy transfer from secondary to primary were accounted for in the detailed model. The hot legs included five heat transfer nodes in the wall to accurately predict the wall heat transfer which was found to be important in the integral-model calculation. A schematic of the loops for the detailed model is shown in Figure 32.

The core and upper plenum, along with the lower plenum and downcomer, were modeled with the three-dimensional vessel component of TRAC. A vessel noding diagram is given in Figure 33. A total of ten axial levels were included along with four azimuthal sectors and four radial regions for a total of 160 mesh cells.

This noding scheme is the evolution of several attempts to model the system using a minimum number of mesh cells without compromising the calculation. Originally, the core region contained three axial levels and the lower plenum contained only one axial level. It was determined that an additional level was required in both regions to best simulate the reflood process. Also, originally the downcomer was modeled with one dimensional components. Uncertainty with respect to the connections between the 3-D lower plenum and the 1-D downcomer led to the addition of a fourth radial ring to model the downcomer.

The outer radial region in the core included the blockage due to the barrel-baffle. The radial non-uniformity of holes in the UCSP along with the non-uniform distribution of SCs and GTs in the upper plenum were also accounted for. A single pipe component connected the top of the core to the top of the downcomer. This

pipe represented the flow path through the SCs and GTs into the upper head and through the cooling jets to the downcomer. By connecting the pipe directly to the downcomer (with appropriate loss coefficients), separate modeling of the upper head and cooling jets was avoided. The hot legs and LPI lines all connect into different azimuthal sectors of level nine in the upper plenum. It was not necessary to connect the LPI lines one level below the hot legs as in the integral model because an adequate number of azimuthal sectors existed to accommodate all the connections.

The possibility exists that LPI liquid can be channeled to the peripheral regions of the core by the structure (SCs and GTs) present in the upper plenum. This would allow the LPI liquid to flow to the lower plenum with a minimum amount of interaction with the core. With a finite-difference code such as TRAC, only average flow area fractions and volume fractions are input to model structure. The impingement of a liquid jet on a local flow blockage is not explicitly modeled. Therefore, very large artificial values of friction were applied to the liquid phase in the radial direction at the elevation of injection (the outer radial face of cells 6 and 8, level 9 in Fig. 33). This represents a bounding case in which the LPI liquid is not allowed to penetrate radially into the upper plenum, but instead is forced to travel azimuthally or vertically in the outer radial region of the upper plenum in level 9. It did not seem reasonable to restrict radial flow on the UCSP, level 8.

A steady-state radial power profile was chosen in which the power peaked in the inner radial region as shown in Table VI. This power distribution would tend to favor preferential flow in the outer radial region. The axial power shape was identical to that of the integral model.

Table VI: Steady-State Radial Power Profile

Core Region	Relative Power Factor	Average Linear Power (kw/ft)	Peak Linear Power (kw/ft)
1	1.1	6.58	9.31
2	1.0	5.98	8.47
3 (outer)	0.9	5.36	7.62

The results from the integral model at 30 s were used to provide initial conditions for the detailed model starting at the beginning of the reflood phase of the accident. To initialize the conditions at 30 s for the detailed model, both spatial and temporal averages of the integral-model results were necessary.

Spatial averaging was straightforward for the situation in which the integral model contained more cells than the detailed model (such as in the loops). However, where the integral model contained fewer cells than the detailed model (such as in the vessel), insufficient information existed to provide all the required input for the detailed model. For example, the detailed model contains three radial regions in the core compared to only one radial region for the integral model. The detailed model, therefore, requires radial-dependent input that is not provided by the integral model. For this reason and to simplify input, it was decided to initialize all liquid and vapor velocities to the value of zero in the detailed model. This, however, had the effect of "throwing away" the initial motion of the fluid and made it necessary to input the initial liquid inventory based on time-averaged values. For example, oscillations between the downcomer and the core existed during the early part of reflood in the integral-model calculation. The oscillations resulted in some of the downcomer liquid being pushed out the break. If the downcomer liquid inventory at 30 s is used for the detailed model along with zero velocities, this mass loss out the break is not accounted for. Also, the loss of fluid out the break during the early part of reflood is not accounted for because the initial momentum of the fluid going out the break is lost when the initial velocities are set to zero. To avoid these problems, the average downcomer and core inventories for the initial period of reflood were input instead of using the instantaneous values at 30 s.

The spatially-averaged pressure at 30 s for the entire integral-model system (including the vessel and loops) was used throughout the detailed model. This pressure was adjusted to account for the gravitational head at the different elevations of the system. Temperatures were adjusted in the detailed model to ensure conservation of stored energy between the integral and detailed models.

Additionally, in the detailed model, the core decay power was linearly ramped from 6.5 MW at 30 s (the calculation starting time) to 65 MW at 30.5 s and the HPI and LPI flows were initiated at 30.5 s. These short delays allowed time for the fluid velocities and heat-transfer coefficients to become established and helped to avoid any numerical instabilities that might occur when trying to start "in the middle" of a highly turbulent, non-equilibrium transient. It was also necessary to suppress subcooled boiling for the first few seconds to prevent numerical instabilities. This strategy for initializing the detailed-model calculation worked well and produced a reasonable simulation of reflood compared to the integral-model results.

3.2 Detailed Model Transient Results

3.2.1 Calculation Assumptions

The calculation assumptions are the same as those used for the integral-model calculations (see section 2.2.1). However, only the reflood phase of the transient (starting at 30 s) is simulated using the results from the integral model as a basis for determining initial conditions. Again, two cases were performed: case UPI' assumed LPI into the upper plenum and case DI' assumed LPI into the downcomer.

3.2.2 Comparison of Case DI' and Case DI

The results for case DI' agree well with the integral-model results, case DI. The vessel and core liquid levels increased at approximately the same rate for both cases. Manometer oscillations between the core and downcomer occurred in the integral-model calculations as mentioned in section 2.2.3. These oscillations also occurred in the detailed-model calculations, but to a lesser extent. The smaller oscillations were probably due to the increased number of degrees of freedom in the core for flow. The result of the smaller oscillations was a somewhat higher reflood rate because of a decrease in the amount of fluid lost out the break. This difference was small, however, and did not significantly alter the progression of the transient.

The PCT was reached at about the same time (70 s) for both cases as shown in Figure 34. The slightly higher PCT for case DI' (960 K compared to 940 K for Case DI) is primarily a result of the peaked radial power profile. Recall that the detailed model contained three radial core regions with the power peaked in the inner region. Figure 35 shows the clad temperature for an average rod in each of the three radial regions at the 2.28 m core elevation and demonstrates the effect of the radial power profile.

Case DI' was terminated at 130 s into the transient. In general, the results for case DI and DI' are the same; 3-D effects in the core do not have a substantial influence on the progression of the transient when LPI is injected into the downcomer. Case DI', therefore, serves as a reference case for investigating the effects of upper plenum injection.

3.2.3 Comparison of Case UPI' and Case UPI

Again, the results from the detailed model and the integral model are very similar. However, 3-D effects in the core and upper plenum were found to be significant.

A pool of subcooled liquid formed on the UCSP in the detailed-model calculation as it did in the integral-model calculation because of the occurrence of a CCFL condition. This pool was somewhat smaller, however, as shown in Figure 36, which shows the upper plenum liquid volume fraction for cases UPI and UPI'. The reason for the smaller pool is that the LPI liquid was better able to penetrate the UCSP; i.e., only partial CCFL occurred in the outer radial region of the core.

The lower power (and related lower vapor velocities) in the outer radial region of the core favored penetration in that region. Recall that the LPI liquid jet was artificially restricted from flowing radially at the location of injection. This also greatly enhanced LPI penetration in the outer radial region.

In addition to case UPI', a short portion of the transient was simulated in which no artificial radial restriction was imposed in the upper plenum. Liquid penetration was again enhanced in the outer radial region (because of the lower power in that region) but not to the extent observed with the artificial restriction. When no artificial restriction was imposed, the results more resembled those of the integral model. That is, the amount of channeling decreased, leading to higher PCTs. This calculation was run only to verify the necessity of modeling a radial restriction to account for the upper plenum internals and was not completed.

Although the LPI liquid jet was restricted from flowing radially at the location of injection in case UPI', it was free to travel radially when it reached the UCSP. The point to be made is that not all of the LPI liquid penetrated the UCSP and that radial flow on the UCSP was, in fact, observed. This led to the liquid pool formation in the upper plenum.

Partial channeling of LPI liquid did occur, however, in the detailed-model calculation. Figure 37 shows the clad temperature at the 1.37 m core elevation for rods 4, 8, and 12. Rod 12, in the outer radial region, quenched much sooner (at 90 s) than the inner rods because of LPI channeling. This rod is located directly beneath the UPI nozzle. Rod 9, adjacent to rod 12, but not directly beneath an injection nozzle, did not quench until 140 s. The effect of channeling was to increase the delivery rate of LPI liquid to the bottom of the core which resulted in an increased bottom reflood rate relative to the integral-model results (case UPI).

Because of the increased bottom reflood rate for case UPI', the maximum average-rod temperature, shown in Figure 38, was lower by approximately 30 K at the time the PCT occurred (about

160 s for both cases). Recall that the peak linear-power-generation rate for case UPI was 8.72 kw/ft compared to 9.31 kw/ft for case UPI' so that a direct comparison of PCTs is not strictly legitimate. The lower PCT for case UPI' (even with a higher peak linear-power-generation rate), however, demonstrates the importance of LPI liquid channeling.

Figure 38 also shows that, at approximately 92 s, a sharp drop in the clad temperature occurred for case UPI'. This resulted when a large slug of liquid from the upper plenum reached the steam generators. Secondary-to-primary heat transfer vaporized the slug of liquid and led to a large pressure pulse. The pressure pulse was unrealistically large because of the very coarse noding in the steam generator (only two cells). In the integral-model calculation, the steam generator was modeled with twelve cells. When a slug of liquid reached the SG in that model, a small pressure increase occurred in the first couple of cells. This pressure increase prevented the slug from further entering the SG. However, in case UPI', when the slug of liquid entered the large cells in the SG, the available wall area for heat transfer to the liquid was very large and resulted in complete vaporization of the slug. The pressure pulse was large enough to push most of the liquid from the downcomer and upper plenum into the core. Rapid cooling of the fuel cladding occurred and the subsequent vapor generation led to another pressure pulse which forced much of this liquid back out of the vessel.

The vessel liquid mass for cases UPI and UPI' is shown in Figure 39. Recall that in the integral-model calculation a level swell was beginning at around 100 s when the downcomer and lower plenum liquid was heated to saturation by the hot vessel walls. This effect also occurred in the detailed-model calculation but was initiated about 8 s sooner because of the unrealistic SG pressure pulse. The result was that about the same amount of liquid was lost from the vessel and about the same amount of energy was removed from the vessel walls for both cases. However, the pressure pulse did momentarily enhance the cooling of the fuel cladding for case UPI'; because the pressure pulse lasted only two or three seconds, very little of the fuel stored energy was removed and none of the fuel rods were quenched.

It would be necessary to rerun the entire calculation with a modified SG model to determine the exact consequences of the pressure pulse. Limited time and computer resources prevented this. However, a small portion of case UPI' was rerun (from 90 to 100 s) with the SG heat transfer suppressed to prevent the unrealistic pressure pulse. The system response was very similar to that of the integral-model calculation and helped to verify that the SG pressure pulse did not significantly affect the outcome of the transient. Except for the channeling of LPI liquid, case UPI' demonstrated the same response as case UPI.

3.2.4 Comparison of Case UPI' and Case DI'

The hot-leg responses for cases UPI' and DI' differed because of the horizontal entrainment of LPI liquid from the upper plenum in case UPI'. The effect was the same as that predicted by the integral-model calculations; some of the LPI cooling availability was lost to the hot-leg metal mass.

The difference in the vessel response between cases UPI' and DI' is demonstrated by the clad temperature histories. Figure 40 shows the clad temperature for an inner rod, number 4, at the 1.37 m elevation for both cases. (Core midplane is at the 1.83 m elevation.) This position quenched much sooner for case DI' because of the faster-moving bottom-flood quench front for that case.

Figures 41 and 42 show the clad temperature at the same elevation for rods 8 and 12, respectively. Rod 8 is in the center radial region and rod 12 is in the outer radial region directly below an upper plenum injection nozzle. The inner and outer rods for case DI' are seen to quench at about the same time. (The outer rod quenched about 12 s earlier because of the lower power in that region.) For case UPI', however, the rod in the outer radial region quenched about 80 s earlier than the inner rod. This demonstrates the strong effect of LPI liquid channeling in the outer radial region.

Figure 43 shows the clad temperature in rod 9. This rod is also located in the outer radial region, but is not directly beneath an UPI nozzle. This rod quenched only 35 s earlier than the inner rods and demonstrates the predominance of channeling directly beneath the UPI nozzles.

Figure 44 shows the clad temperature for an inner rod at the core midplane for both cases and also demonstrates the faster moving bottom-flood quench rate for case DI'. Figure 45 shows the clad temperature for an inner rod at the 3.2 m core elevation (near the top of the core) for both cases and illustrates the presence of a falling-film quench front for case UPI'.

Although strong LPI channeling occurred in the outer radial region, some of the LPI liquid penetrated into the center of the core. It is this LPI-core interaction that slows the advance of the bottom-flood quench front. Figure 46 shows the maximum average-rod clad temperature for both cases. The clad temperature for case DI' peaked at about 70 s at a value of 960 K while the clad temperature for case UPI' did not begin to decrease until around 160 s when it reached a peak of approximately 1000 K. (The hot-rod PCT was 1010 K for case DI' and 1080 K for case UPI'.) Although channeling was effective in reducing LPI-core interaction, UPI proved to be less effective than DI with respect to PCT.

Figures 47 through 57 show schematically the movement of liquid in the 3-D vessel during the transient. The intensity of the shading in each cell is directly proportional to the liquid volume fraction for that cell. These figures are intended to give a qualitative insight into the transient. It should be noted that each figure represents a "snapshot" in time for a highly turbulent system. The various snapshots were chosen in an attempt to illustrate the general trend of the transient. Also, the liquid-full regions in the lower plenum do not appear to be fully shaded as intended because of deficiencies in the reproduction process. It is believed, however, that one can still appreciate the figures, especially those showing liquid in the upper plenum and core.

Each figure contains two r-z slices of the reactor vessel. The left slice contains vessel sectors 15, 11, 7, 3, 1, 5, 9, and 13 and the right slice contains sectors 14, 10, 6, 2, 4, 8, 12, 16 (see Figure 33). The right slice, therefore, contains the cells directly beneath the UPI nozzles.

Figures 47 through 50 are for case DI'. The initial conditions for reflood are depicted in Figure 47. Figures 48, 49, and 50 were chosen to demonstrate one cycle of a manometer oscillation between the core and downcomer.

Figures 51 through 57 are for case UPI'. Figure 51 depicts the initial conditions at 30 s and shows the presence of a small liquid pool on the UCSP. One can follow the development of this pool along with its intermittent penetration into the core in Figures 52 through 57. Channeling of LPI liquid can clearly be seen in the outer radial rings beneath the UPI nozzles. This channeling can best be seen in the right slice of Figures 53 through 56.

4.0 COMPARISON TO EVALUATION MODEL CALCULATIONS

Comparing TRAC results to utility or vendor evaluation model (EM) calculations is not straightforward because the TRAC calculations reported herein are based on best-estimate conditions. (The main difference is that EM calculations assume 102% power, 1.2 times ANS decay heat, a 25 s delay on LPI, and only one-half of the available LPI capacity.) The overall response can be compared, however, by comparing the UPI PCT to the non-UPI PCT. Non-UPI refers to the reference case in which LPI is injected into the cold legs or downcomer.

Table VII lists the EM PCTs which were extracted from the final report on the Point Beach LOCA results [2]. These results were obtained by Westinghouse using the 1981 evaluation model with special modifications to account for UPI. The PCTs are shown for varying amounts of core coverage along with non-UPI results. (That portion of the core that is assumed to be in contact with LPI liquid as it travels to the lower plenum is referred to as the core coverage, given as the percentage of total core area.)

Table VII: EM PCTs for Point Beach

	% Core Coverage				
	30	50	70	100	Non-UPI
PCT(K):	1248	1251	1298	1404	1332

The EM calculations indicate that more of the LPI liquid contributes to the bottom-flood quench front as the percentage of core coverage decreases. Conversely, as the percentage of core coverage increases, more vapor is generated and less LPI liquid is available for bottom reflood; hence, higher PCTs result.

The effect of UPI, in terms of a benefit or a penalty compared to non-UPI calculations, is shown in Table VIII for both the cited EM calculations and the current TRAC calculations.

Because of the presence of only one radial region in the core for the TRAC integral model, this calculation can be thought of as having 100% core coverage. Because the LPI was restricted to the outer radial region in the upper plenum (50% of the core area), the detailed TRAC model can be thought of as having approximately 50% core coverage. The detailed TRAC model allows radial flow, however, on the UCSP and where the LPI liquid enters the core so the percentage of core coverage increases as the LPI liquid disperses throughout the core.

Table VIII: Effect of UPI

Calculation	Benefit (+)/Penalty (-) PCT difference (K)
EM, 30% core coverage	+84
EM, 50% core coverage	+81
EM, 70% core coverage	+34
EM, 100% core coverage	-72
TRAC, integral model	-90
TRAC, detailed model	-40

The TRAC integral model calculation and the 100% core coverage EM calculation agree on the effect of UPI; both show large penalties in PCT. The remaining EM calculations, however, all indicate a benefit in PCT for UPI. The TRAC detailed-model calculation predicts a penalty, though smaller than that predicted by the integral model. This supports the contention that LPI channeling is beneficial with respect to PCT, but not to the extent predicted by the EM calculations. This is because the EM calculations do not account for radial flow of LPI liquid on the UCSP and in the core. This radial flow disperses the LPI liquid throughout the core, thereby increasing LPI-core interaction.

5.0 SUMMARY AND CONCLUSIONS

Best-estimate TRAC calculations were performed to investigate large-break LOCAs in two-loop PWRs with upper plenum injection. Two different TRAC models were developed to simulate the transient -- an integral model and a detailed model. The integral model, containing a simple model of the reactor vessel, was used to simulate the entire LOCA sequence. The results of this calculation were used to initialize the detailed model at the time of reflood initiation. This approach proved to be very successful in yielding reasonable results with a significant savings of computer resources.

Both the integral-model and detailed-model calculations predicted higher PCTs when LPI liquid was injected into the upper plenum as opposed to downcomer injection. Horizontal entrainment of LPI liquid and a degraded bottom-flood quench front were found to be the principal reasons for this response.

Horizontal entrainment of liquid from the subcooled pool on the UCSP to the hot legs occurred when LPI was injected into the upper plenum. This cooled the hot-leg walls and resulted in a reduction in the LPI cooling available to the core.

Interaction between the LPI liquid and the top of the core led to vapor generation and decreased the delivery rate of the LPI liquid to the lower plenum. The slower moving bottom-flood quench front resulted in higher PCTs.

Channeling of LPI liquid down the periphery of the core decreased the LPI-core interaction and increased the bottom-flood quench rate. This channeling, however, was not sufficient to decrease the predicted PCT below that of the downcomer injection calculation. A summary of the predicted PCTs for the integral-model and detailed-model calculations is given in Table IX.

Table IX: Summary of TRAC-Calculated PCTs

Case	Average-rod PCT(K)	Hot-rod PCT(K)
UPI	1030	1100
DI	940	1000
UPI'	1000	1080
DI'	960	1010

Because channeling is an important mechanism for enhancing reflood, perhaps better understanding of this phenomenon should be obtained. This understanding can probably be best achieved by performing experiments in large-scale experimental facilities. In addition, the prediction of CCFL across the UCSP, including the effects of radial geometric nonuniformity, is very important and can also be best investigated experimentally.

The use of EM assumptions as opposed to best-estimate assumptions was not explicitly investigated in this study. We believe, however, that the use of EM conditions would result in a greater PCT difference between upper plenum injection and downcomer injection of LPI. The principal reason for the increased difference would be an increase in the amount of LPI-core interaction at the top of the core due to the higher initial power, higher decay power, and reduced LPI flow. Increased interaction would further reduce the delivery rate of LPI liquid to the bottom reflood. Another reason to believe that EM assumptions would lead to a greater PCT difference is that the TRAC-calculated hot-rod PCTs showed a greater PCT difference than the average rod. There is no readily apparent reason for an increased reflood rate to occur when using EM assumptions.

The radial flow restriction in the upper plenum of the detailed model greatly enhanced channeling. Channeling could have been further enhanced by restricting radial flow on the UCSP; this, however, did not seem realistic. It is believed that the detailed-model calculation maximized the degree of channeling and represents a bounding case. (Parametric calculations with different radial power profiles and UCSP geometries were not performed.) Although channeling was effective in reducing the PCT for case UPI', a degraded bottom-flood quench front was observed compared to case DI'.

As described in section 3.2.3, a SG modeling problem resulted in an unrealistic pressure pulse in the core of the detailed model. We believe that this pulse had very little effect on the remainder of the transient because the vessel inventory and the amount of stored energy removed were very close to that predicted in the integral-model calculation. However, if one considers only the results to the time of the pressure pulse (92 s), the PCT for case UPI' is still higher than that for case DI'. Also, the conclusions regarding the effect of channeling remain the same. Therefore, the final conclusions of these analyses are not affected by the SG modeling problem. Based on these best-estimate calculations, upper plenum injection is not as effective as injection into the downcomer.

6.0 REFERENCES

1. Safety Code Development Group, "TRAC-PF1, An Advanced Best-Estimate Program for Pressurized Water Reactor Analysis," Los Alamos National Laboratory Report (to be published.)

2. Attachment in letter from C. W. Fay, Wisconsin Electric Power Company, to H. R. Denton, Director of Nuclear Reactor Regulation, WEP-83-515, "Incorporation of the Westinghouse Model for Upper Plenum Injection in the 1981 Evaluation Model WREFLOOD Code," February 22, 1983.

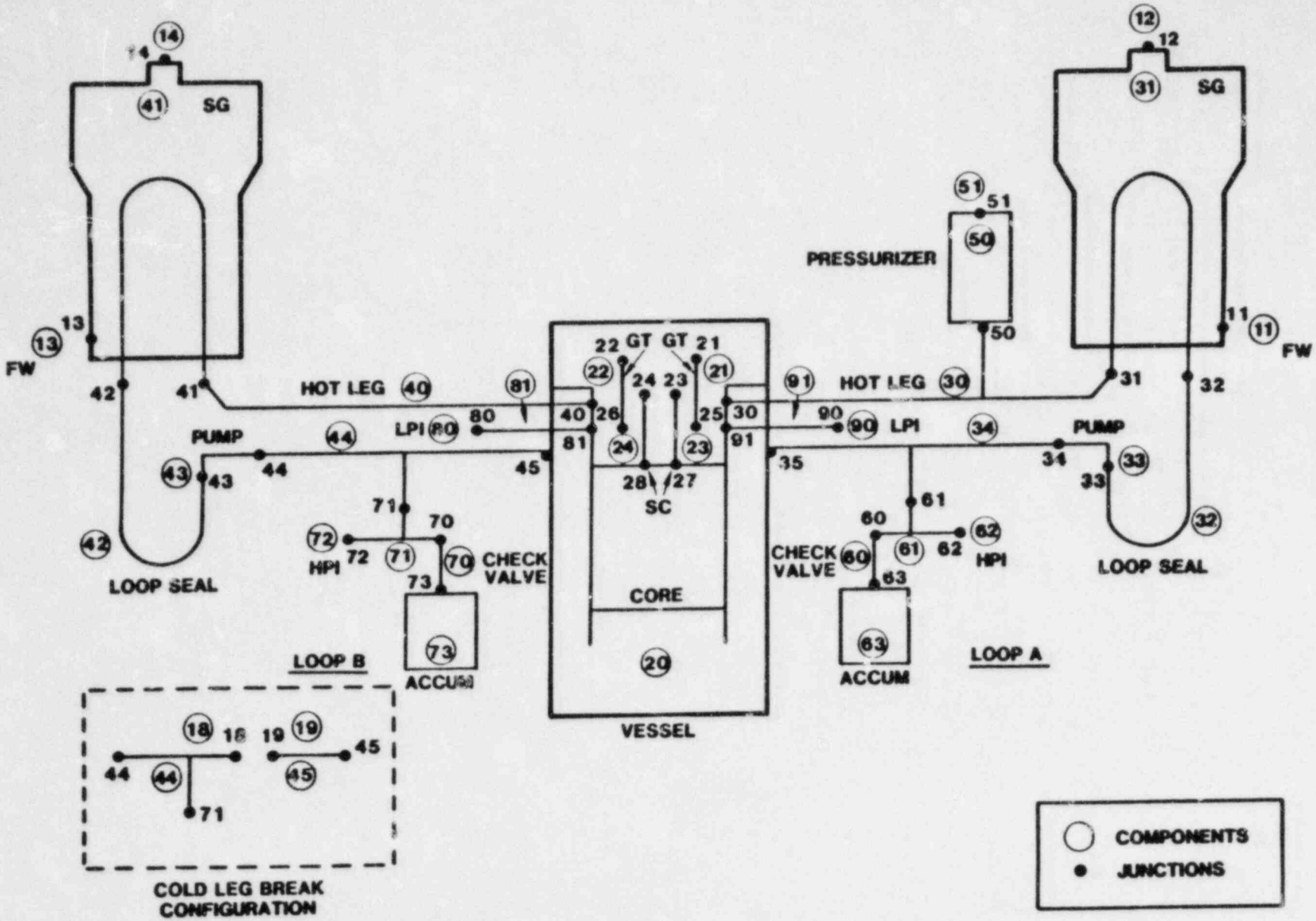

Figure 1. Westinghouse two-loop PWR TRAC schematic, integral model

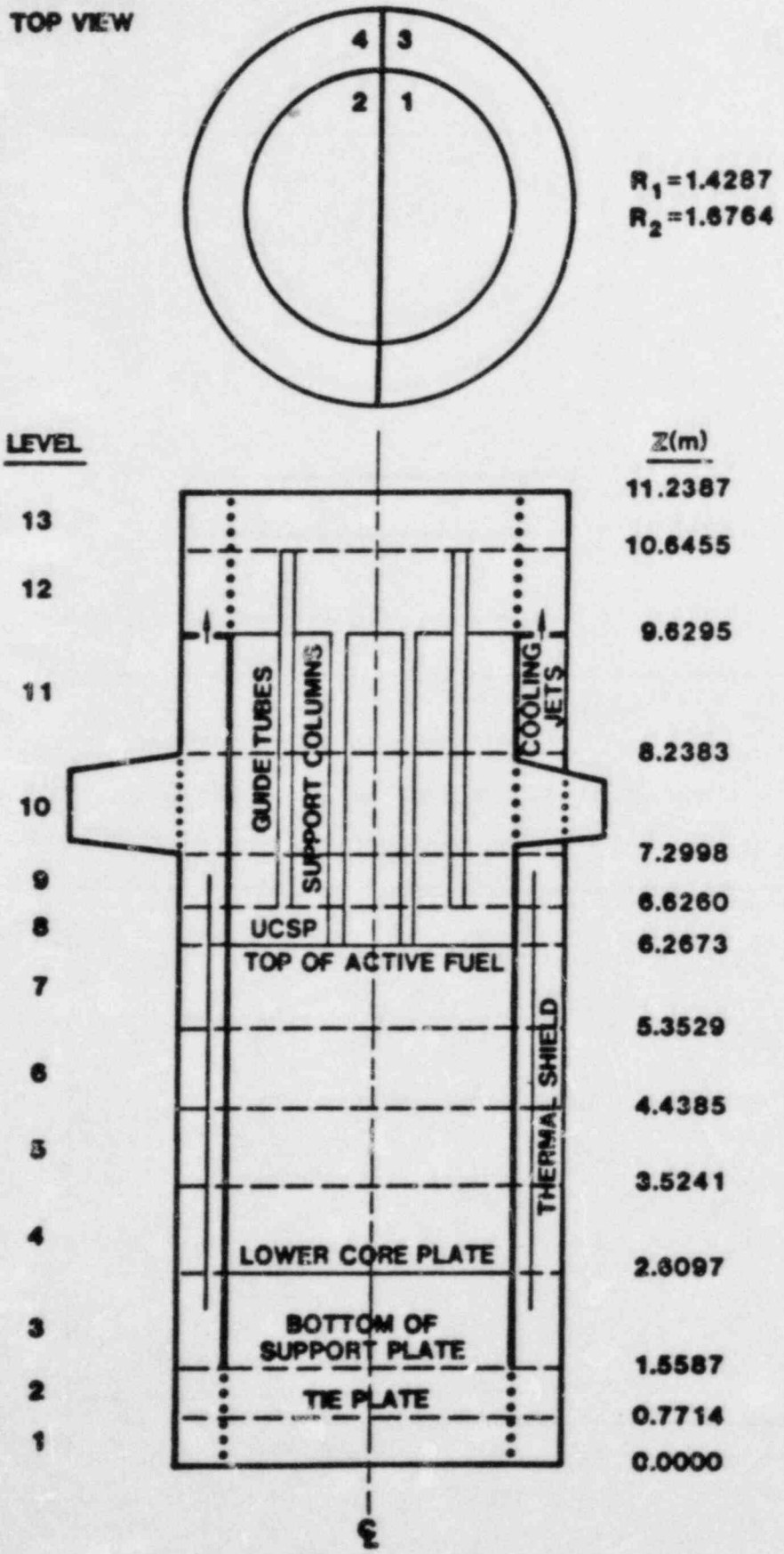

Figure 2. Vessel noding diagram, integral model.

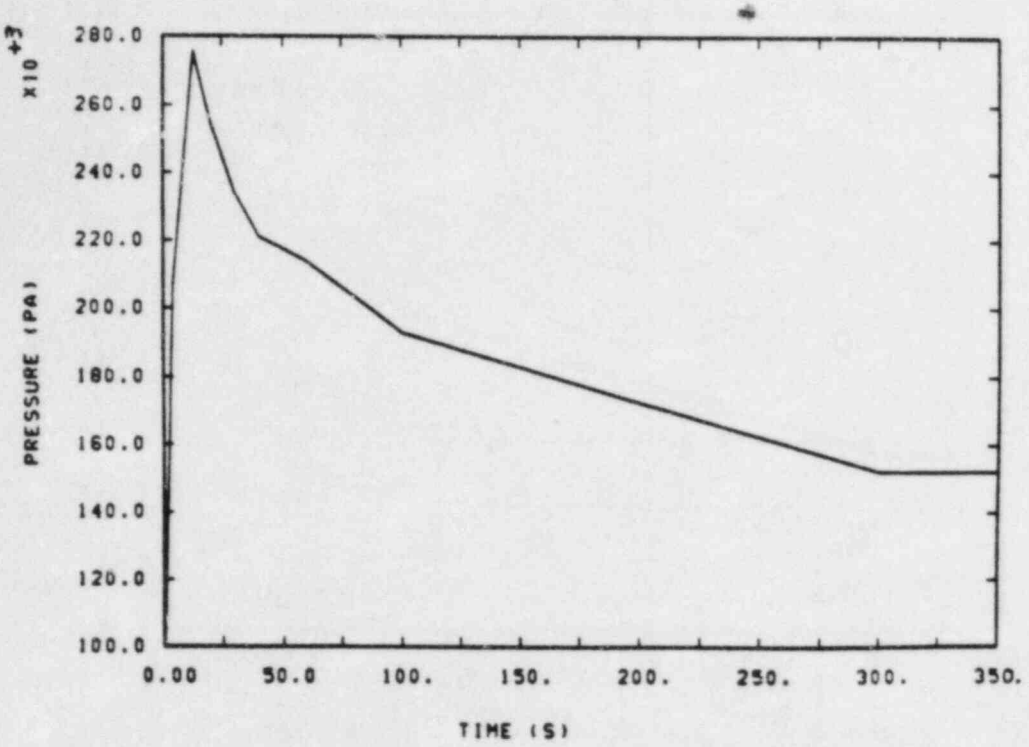

Figure 3. Containment pressure for large-break loss-of-coolant accident.

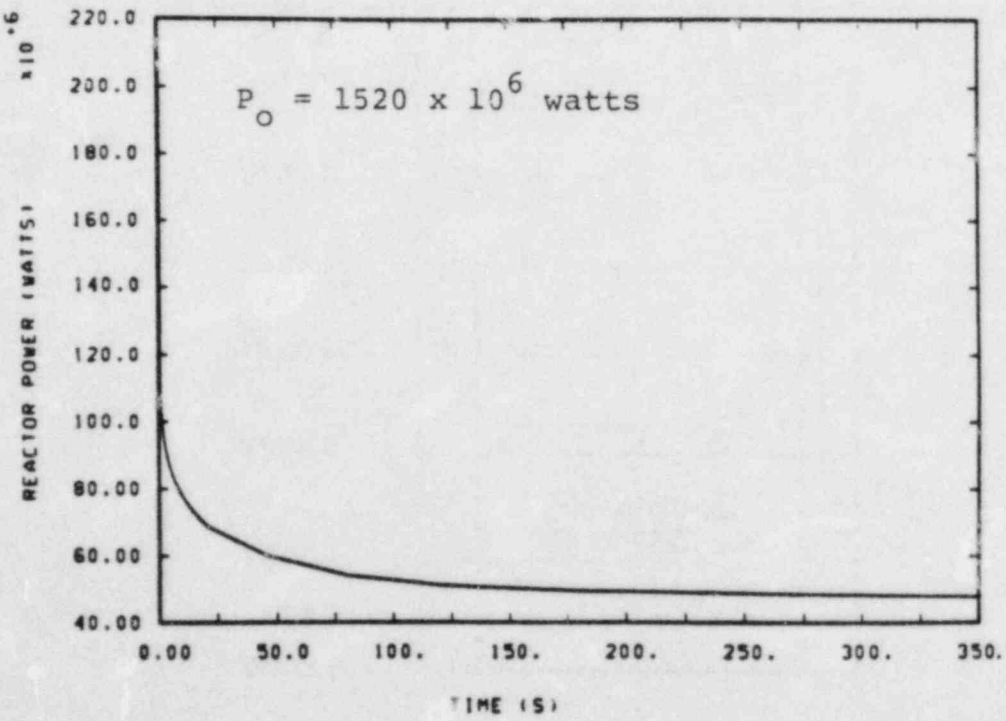

Figure 4. Decay power following large-break loss-of-coolant accident.

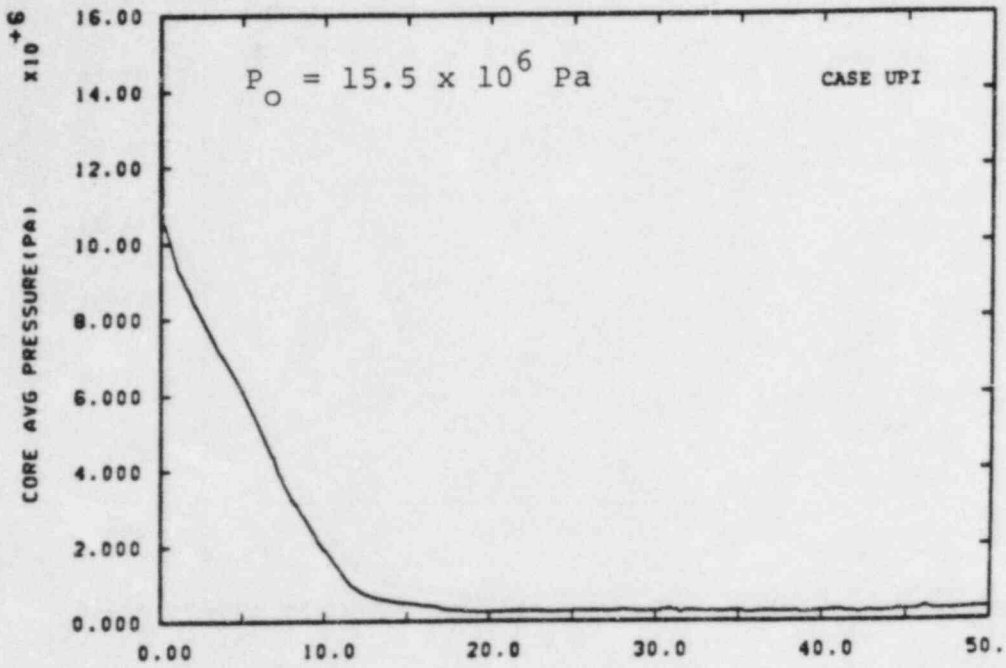

Figure 5. Core average pressure. Blowdown is over at approximately 18 s.

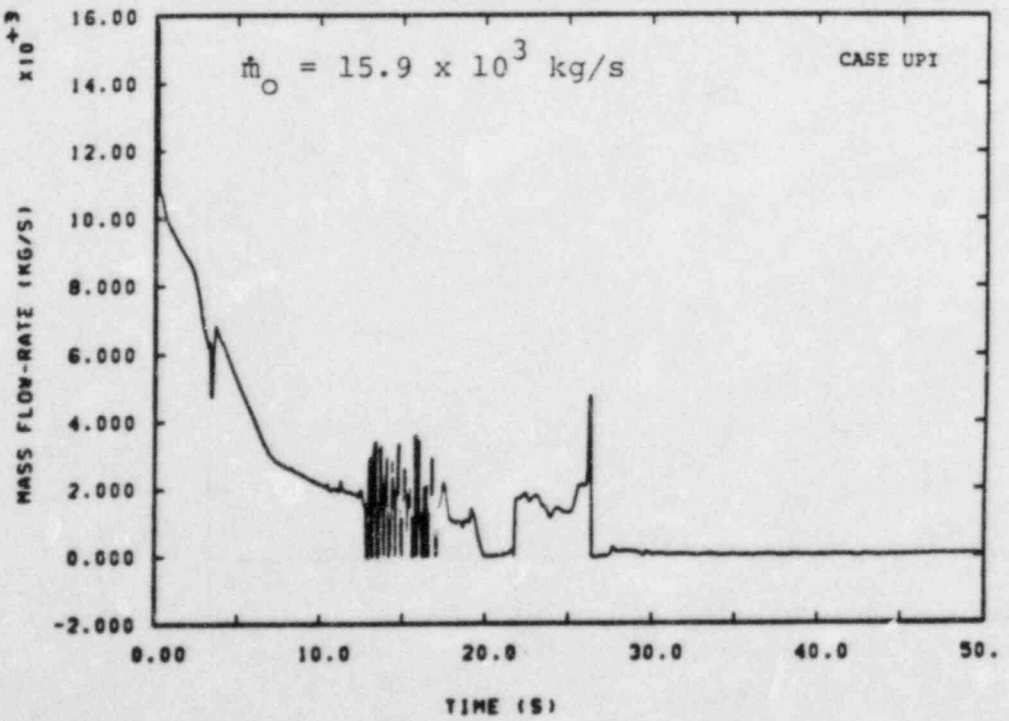

Figure 6. Pump-side break flow.

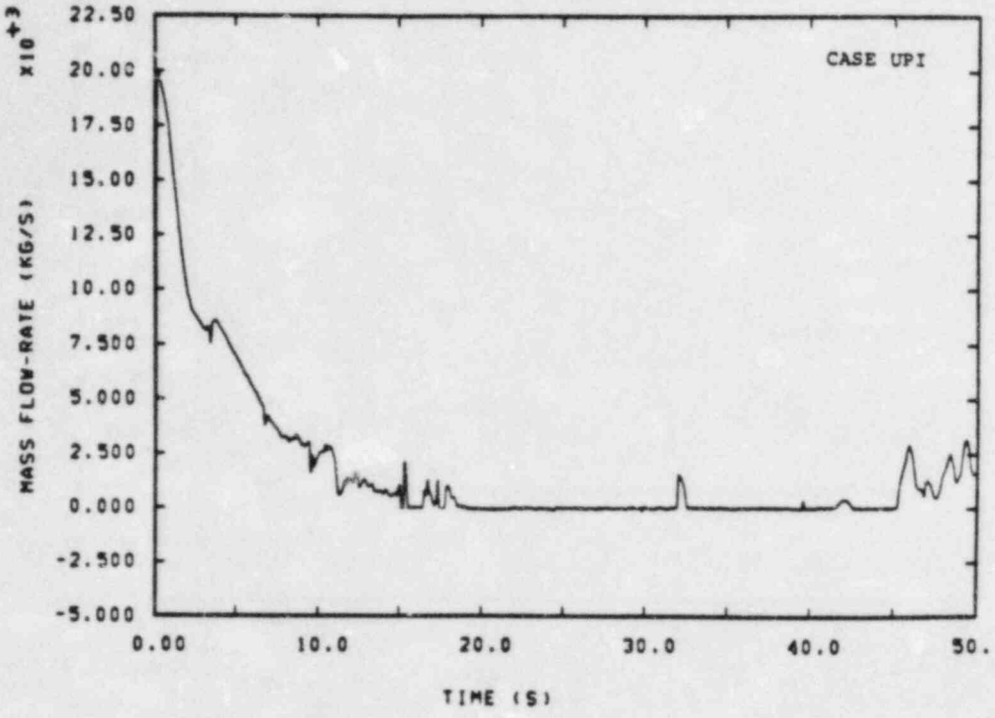

Figure 7. Vessel-side break flow.

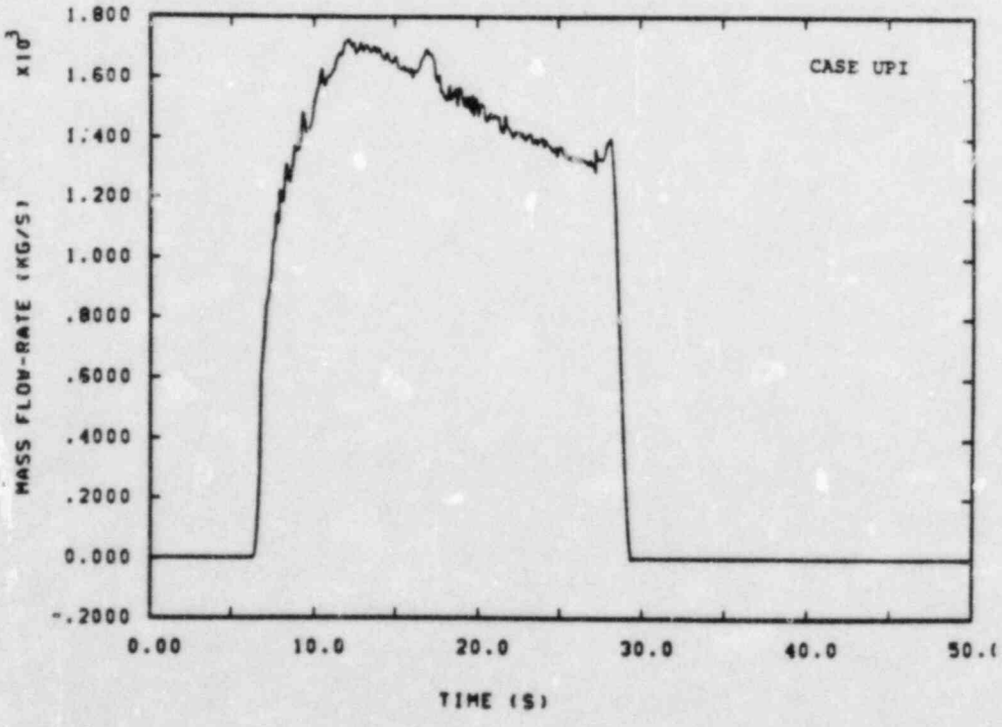

Figure 8. Loop A (intact) accumulator flow. The lower plenum was full at the time the accumulator flow ended.

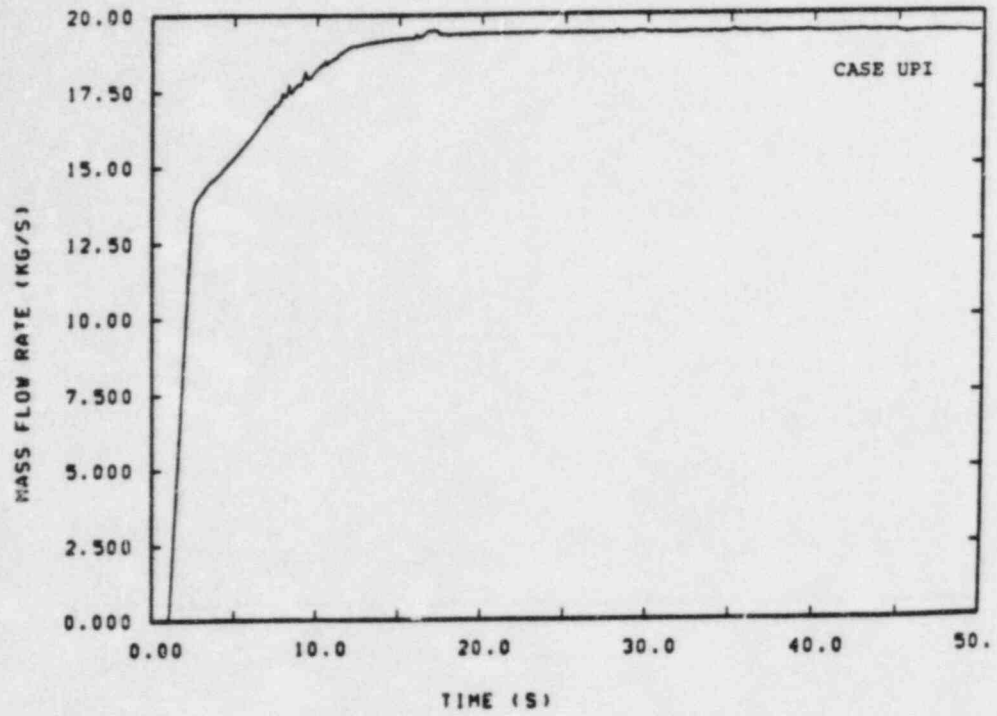

Figure 9. HPI flow (intact loop).

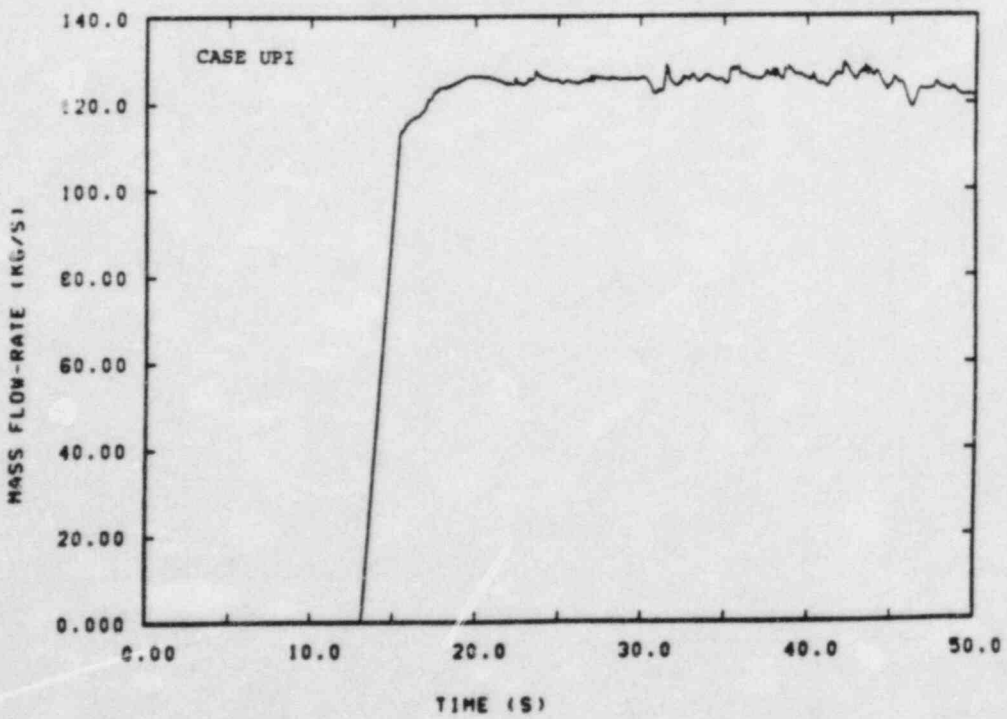

Figure 10. LPI flow (1/2 of total flow).

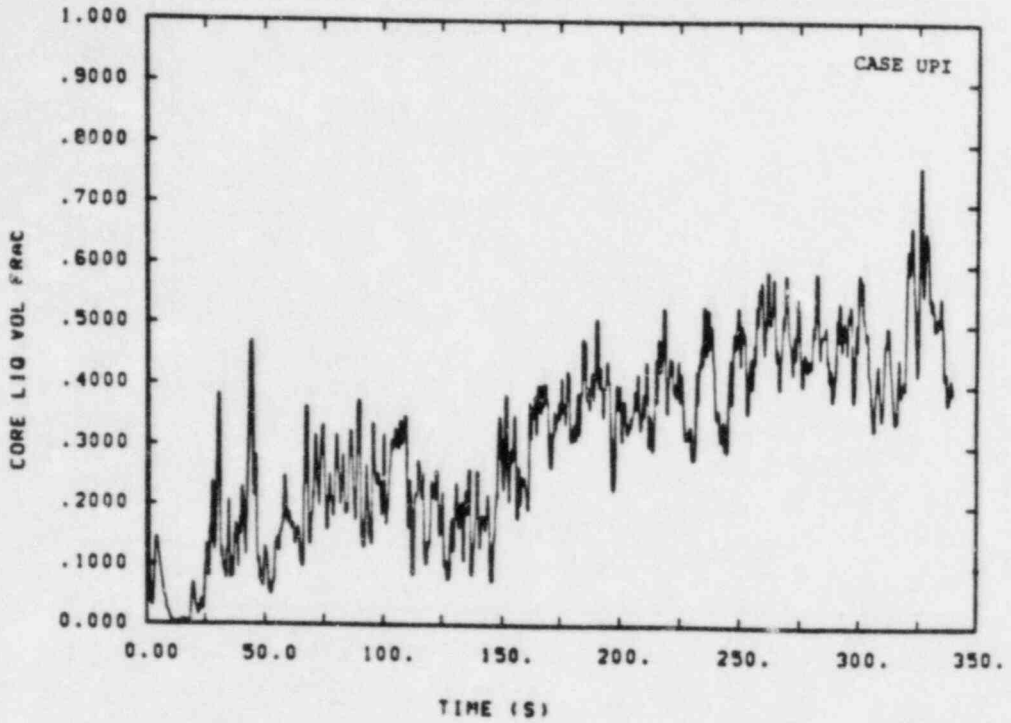

Figure 11. Core liquid volume fraction. The core slowly fills as LPI continues.

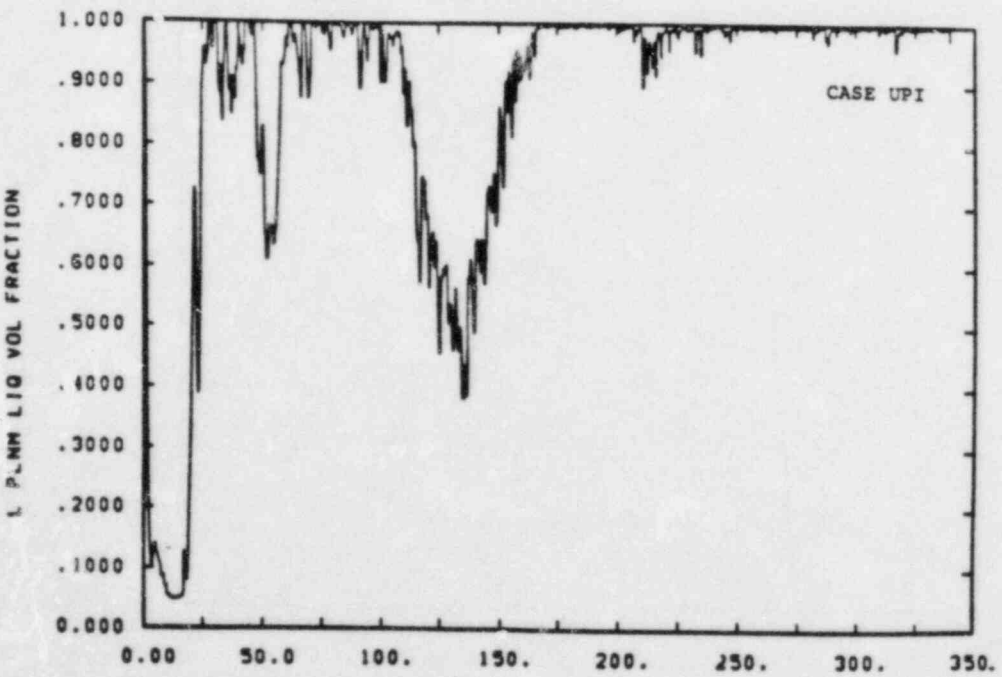

Figure 12. Lower-plenum liquid volume fraction. The lower plenum refills by 30 s.

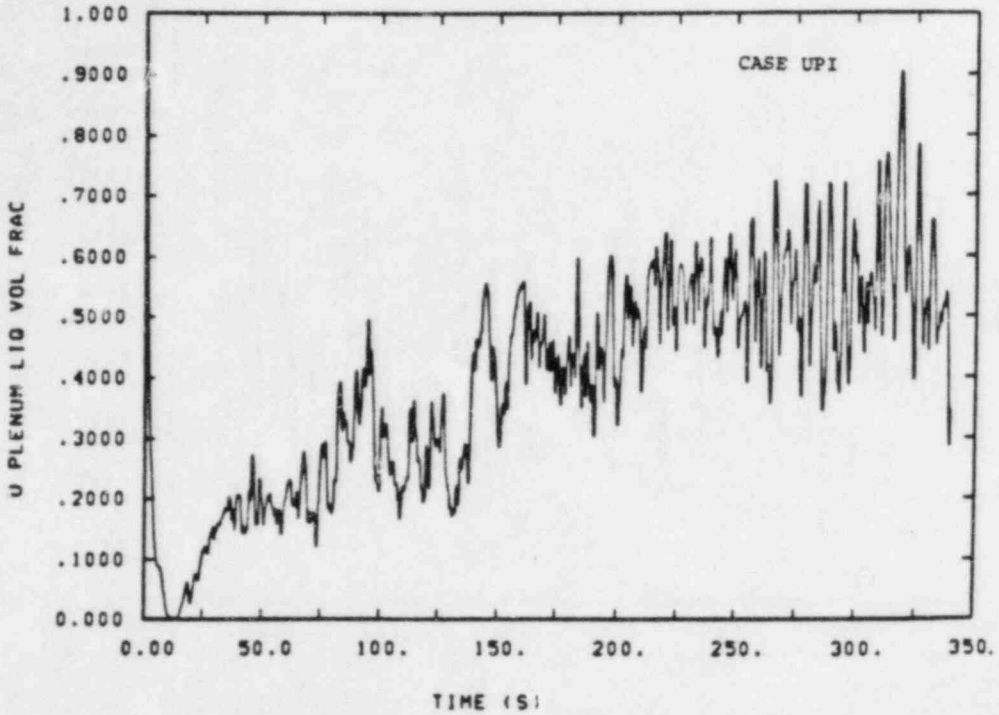

Figure 13. Upper-plenum liquid volume fraction. A large liquid pool formed on the UCSP.

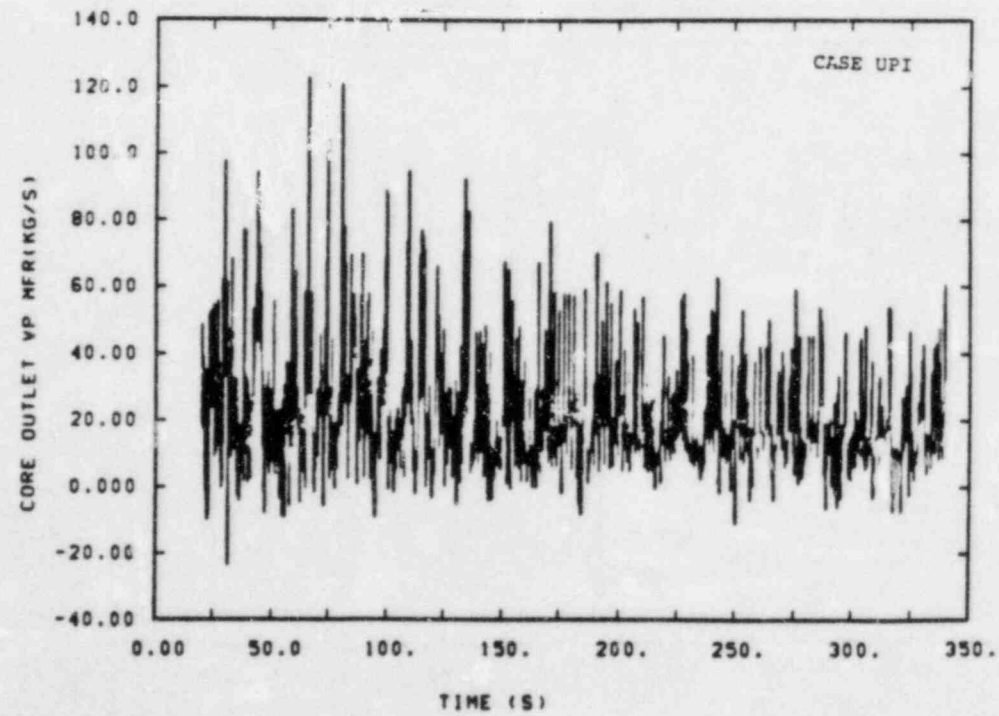

Figure 14. Core-exit vapor mass flow. Vapor generation in the core leads to CCFL.

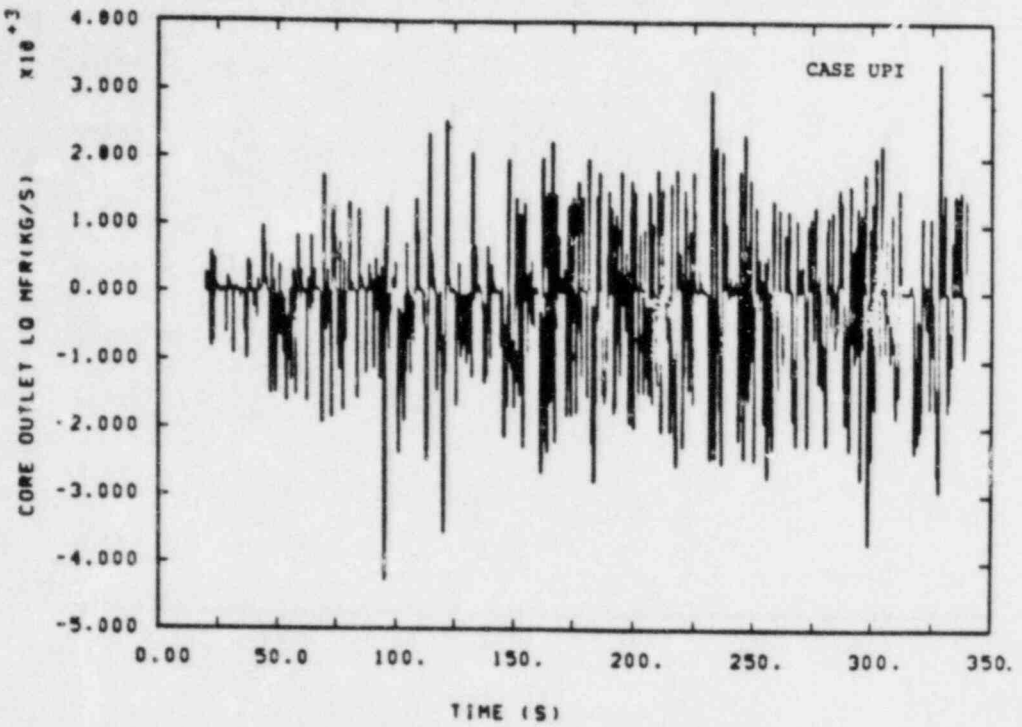

Figure 15. Core-exit liquid mass flow. Intermittent flooding occurs at the UCSP; the net flow of liquid is into the core.

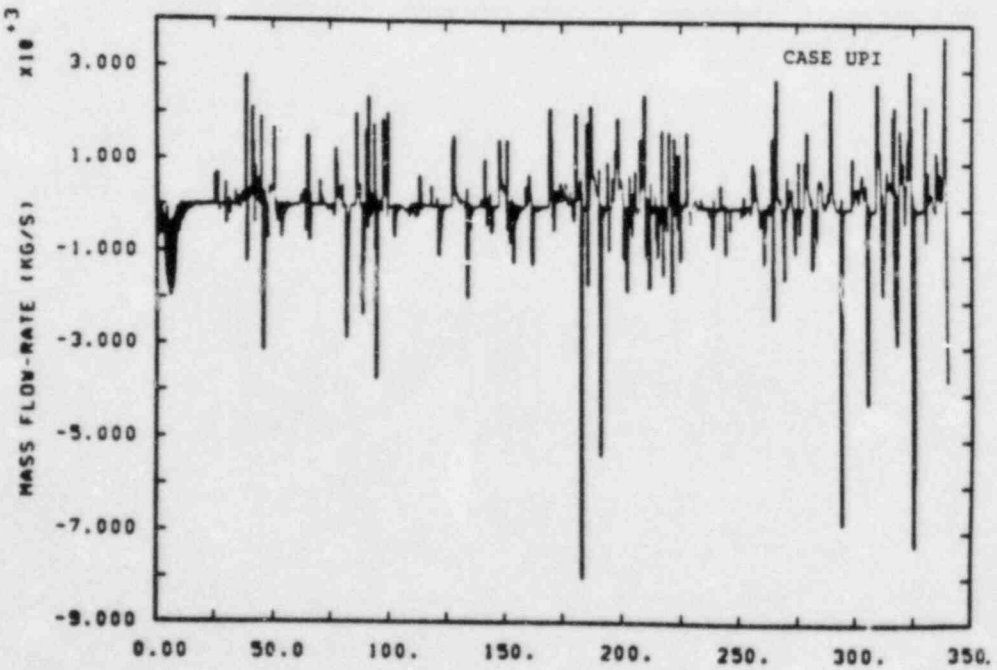

Figure 16. Mixture mass flow into the intact-loop hot leg. Significant horizontal entrainment of LPI liquid from the upper plenum to the hot legs occurs.

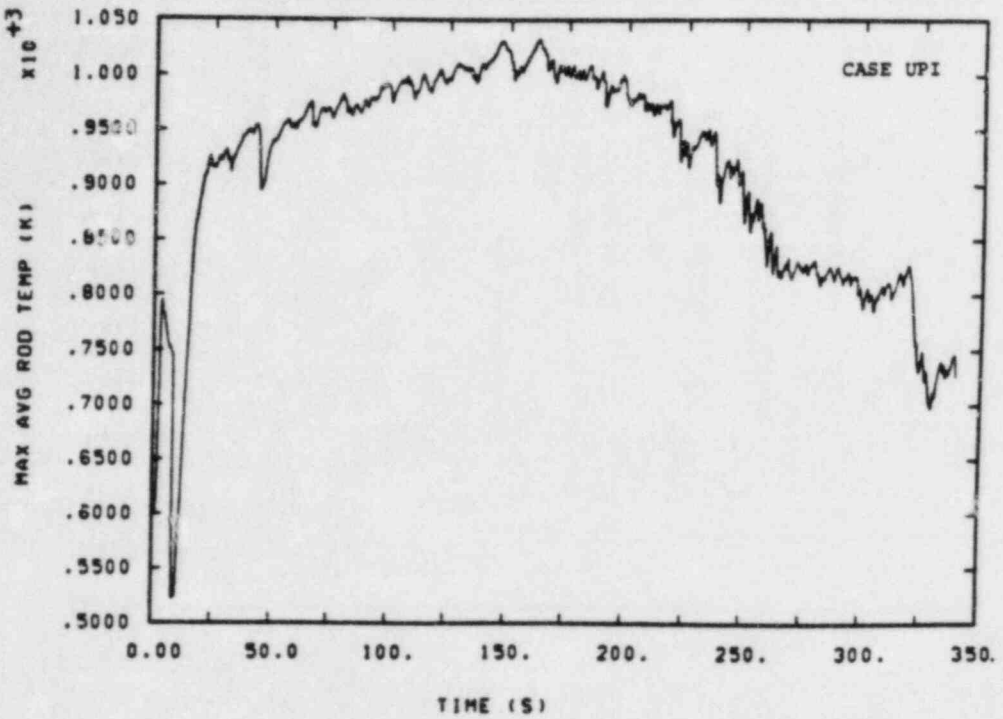

Figure 17. Maximum average-rod clad temperature. PCT reached at 160 s at a value of 1030 K.

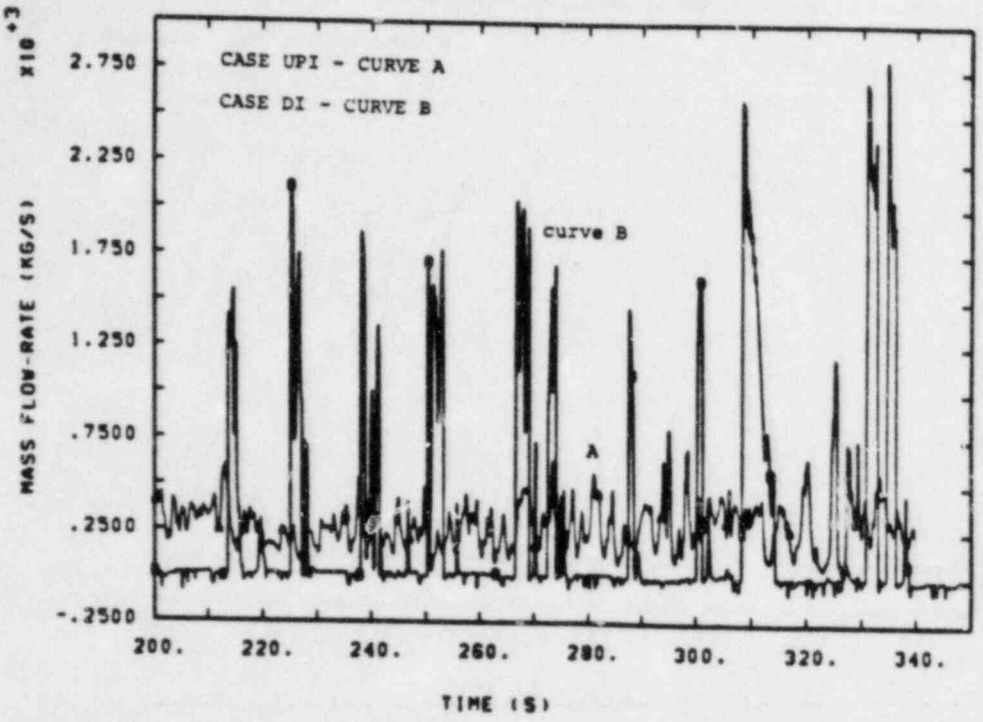

Figure 18. Break mass flow. Manometer oscillations for Case DI result in periodic slug flow out the break.

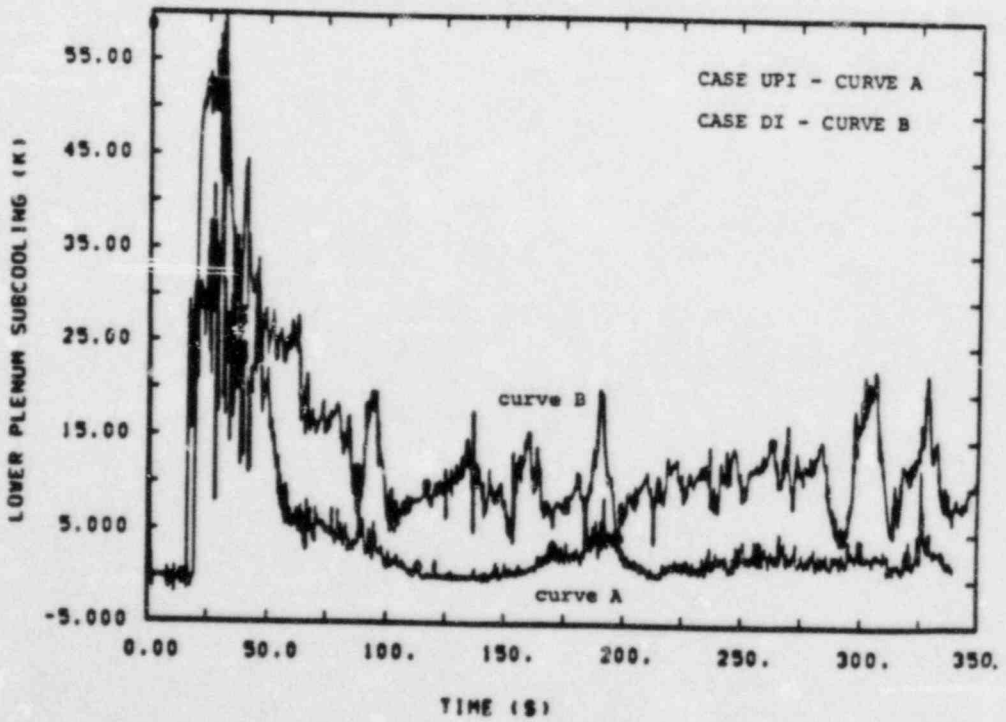

Figure 19. Lower-plenum subcooling. The liquid in the lower plenum remained subcooled for Case DI.

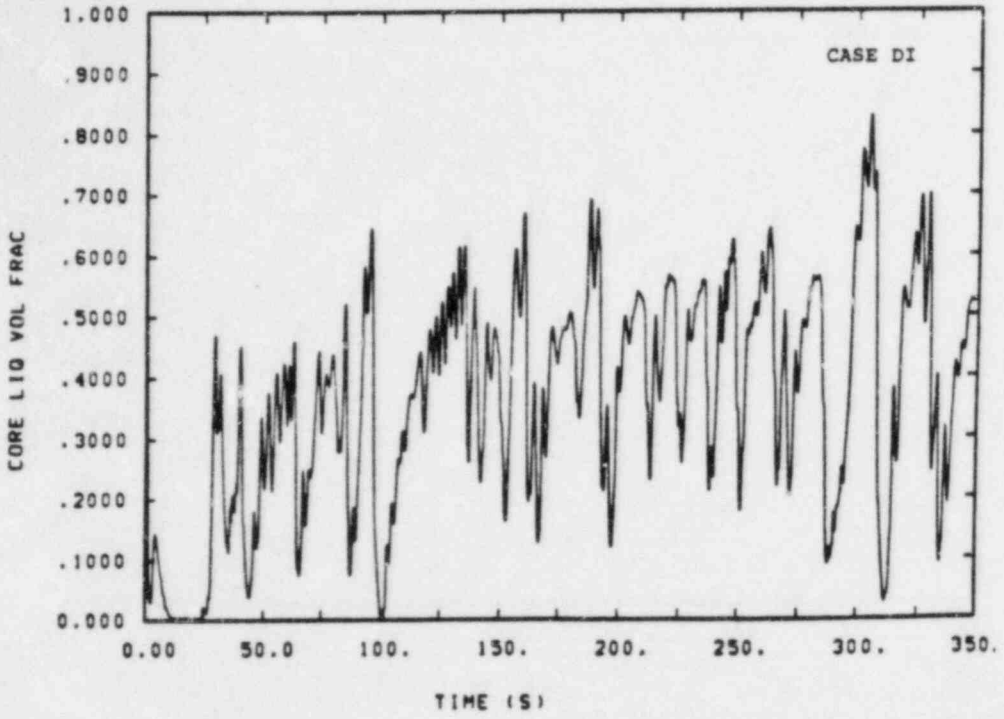

Figure 20. Core liquid volume fraction.

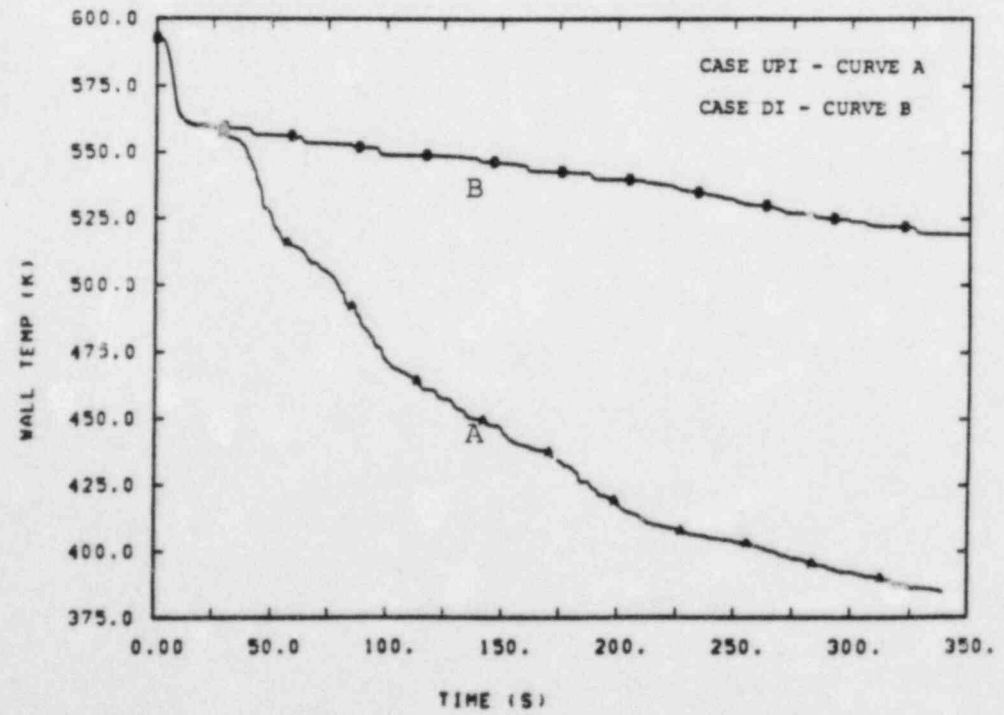

Figure 21. Hot-leg wall temperature. Significant cooling of the hot-leg walls degraded the LPI's core-cooling capacity.

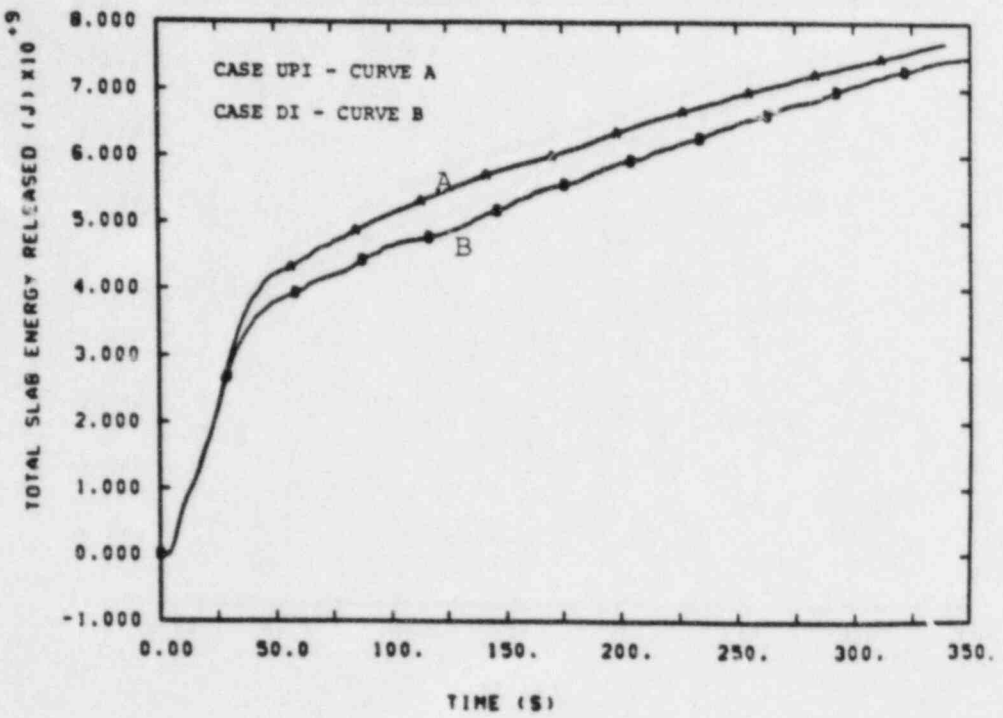

Figure 22. Cumulative energy transfer from vessel structure to fluid.

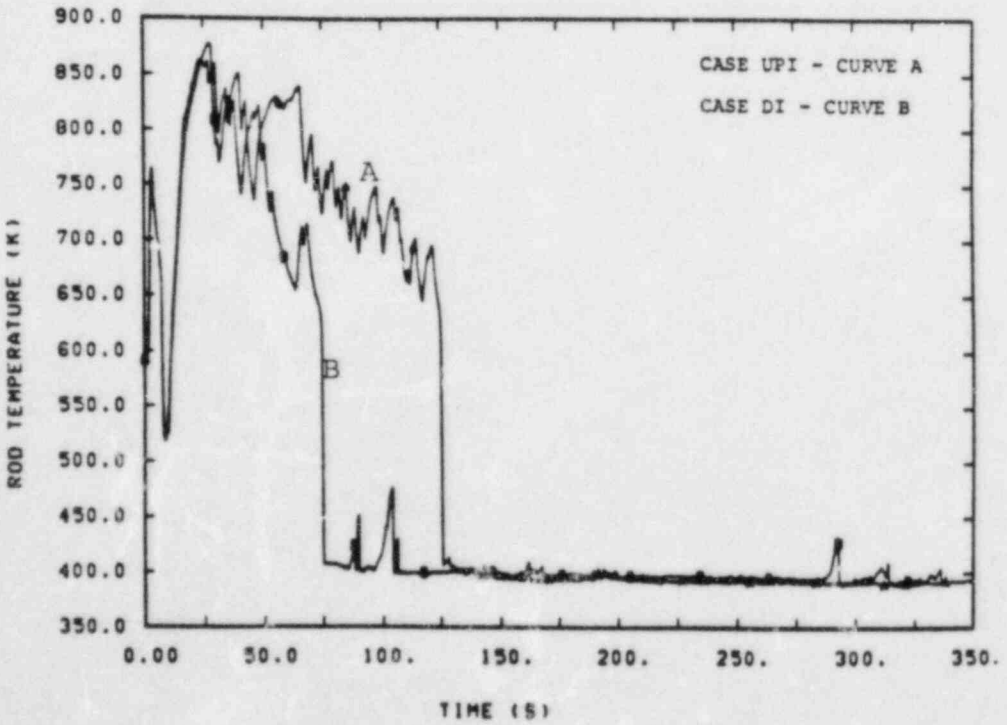

Figure 23. Clad temperature at 0.9144 m core elevation.

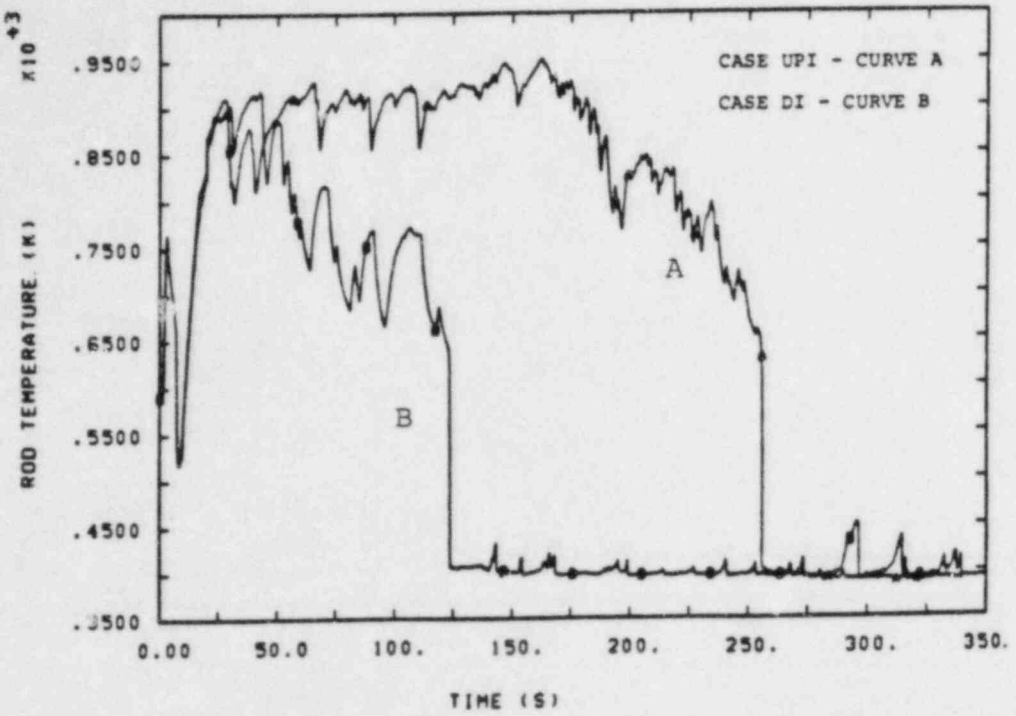

Figure 24. Clad temperature at 1.3703 m core elevation.

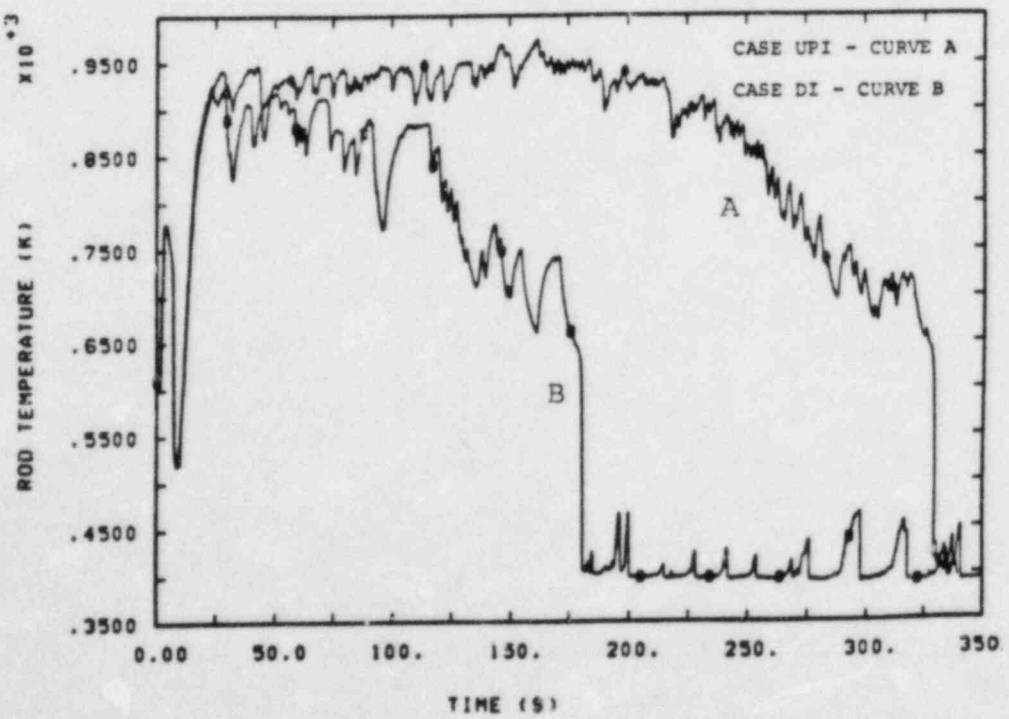

Figure 25. Clad temperature at 1.8288 m core elevation. Quench front takes longer to reach core midplane for Case UPI, resulting in a larger PCT.

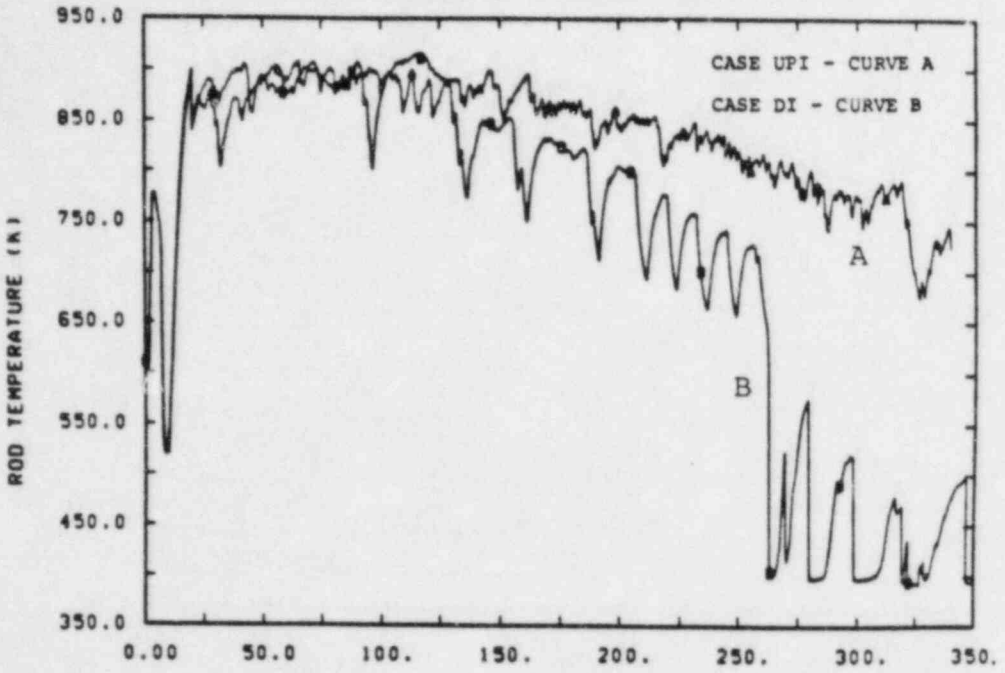

Figure 26. Clad temperature at 2.2803 m core elevation.

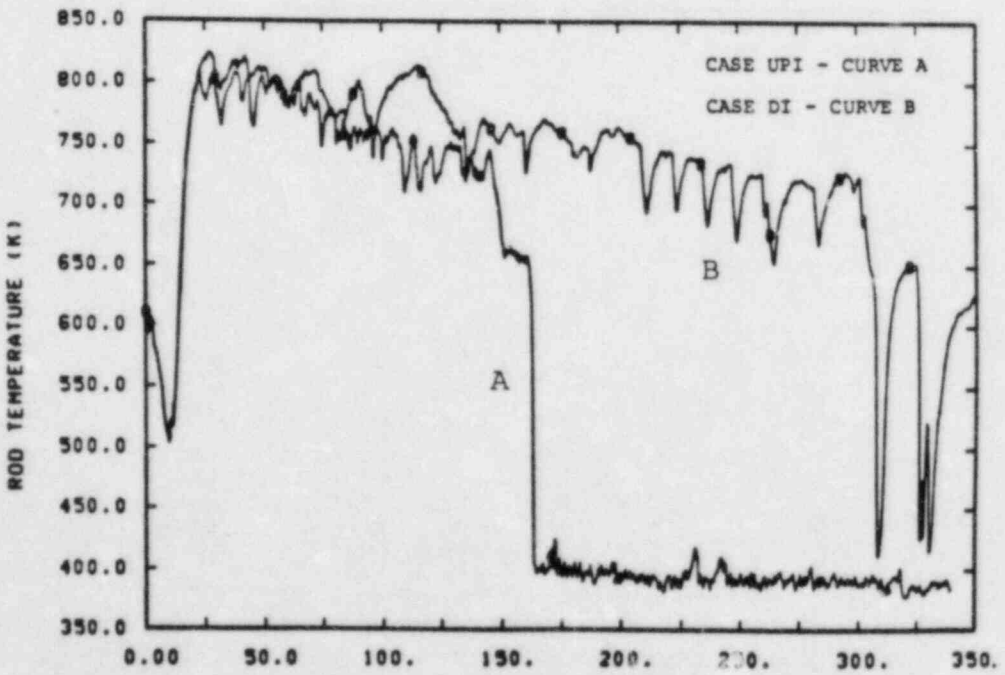

Figure 27. Clad temperature at 2.7432 m core elevation.

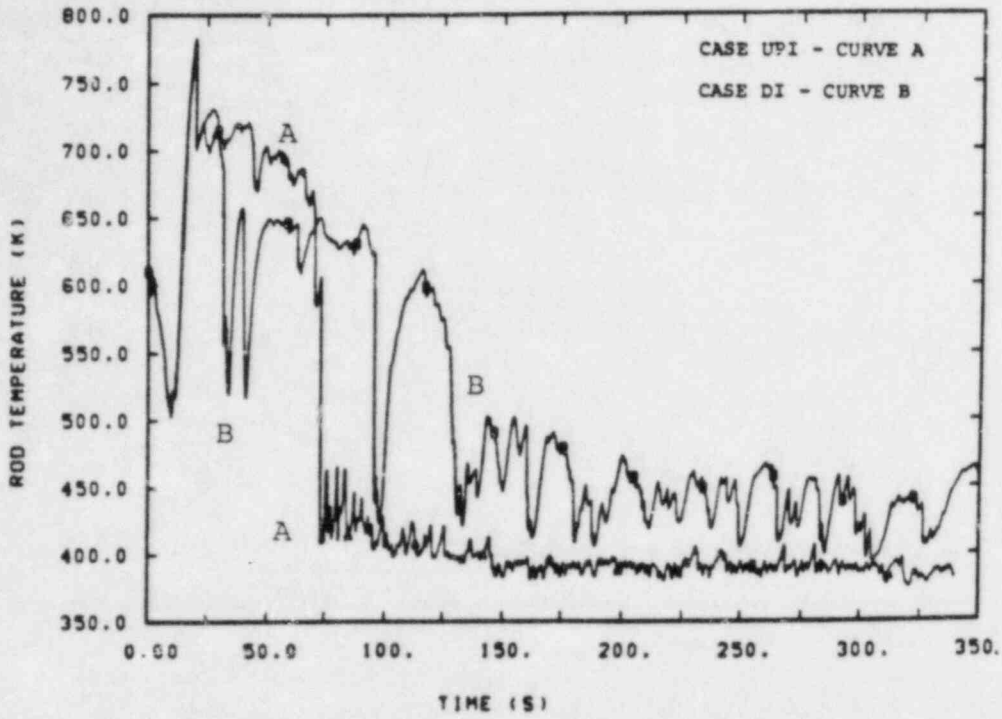

Figure 28. Clad temperature at 3.2003 m core elevation.

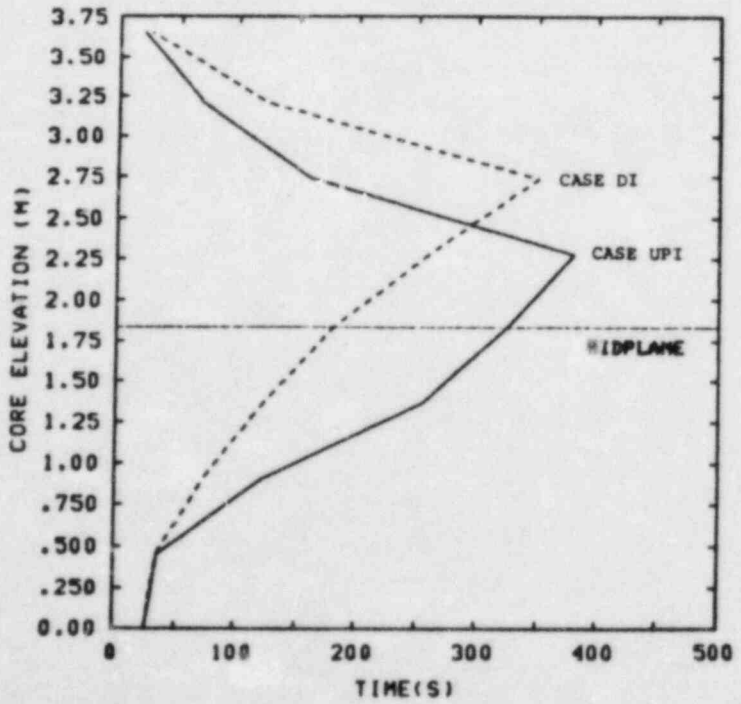

Figure 29. Quench front envelopes. Large falling-film quench front for Case UPI exists at the expense of the bottom-flood quench front.

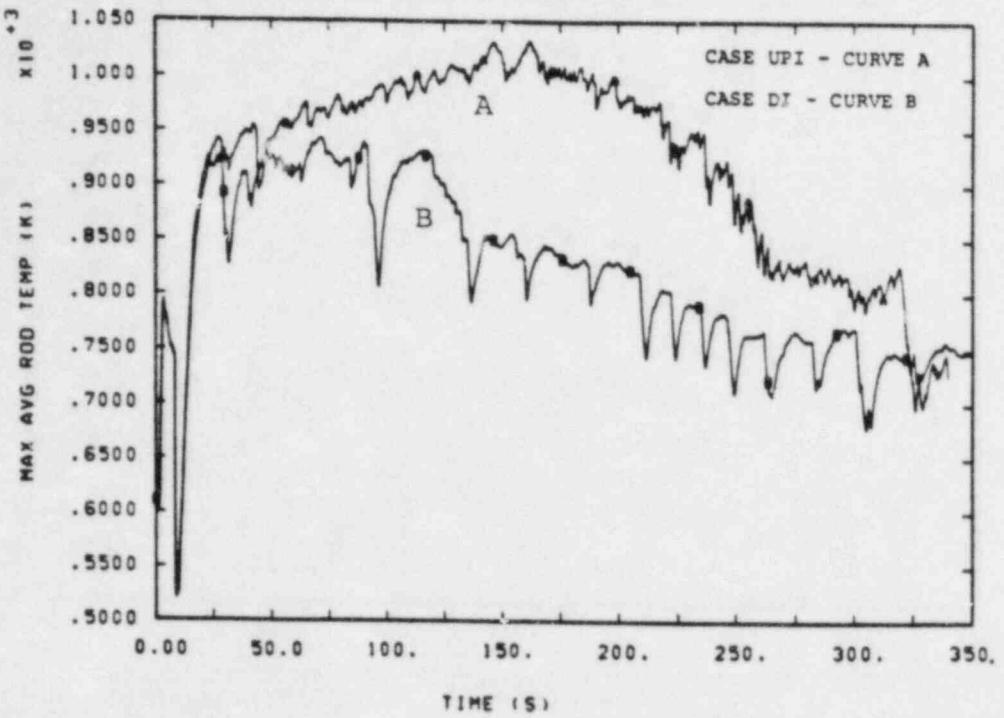

Figure 30. Maximum average-rod clad temperature. PCT remains higher for Case UPI throughout the transient.

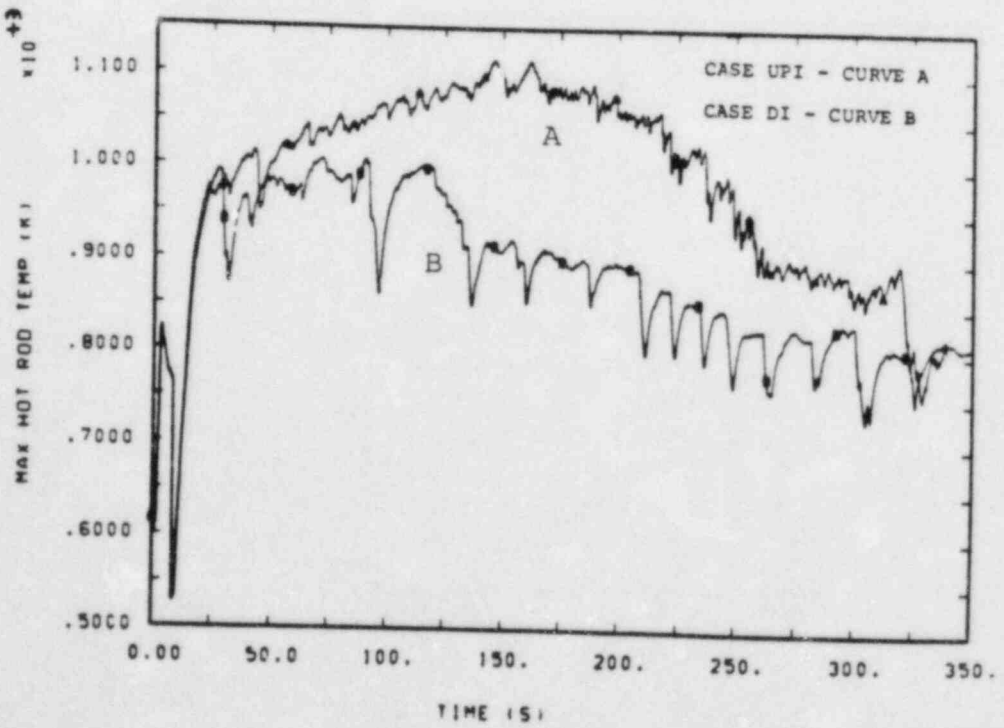

Figure 31. Maximum hot-rod clad temperature.

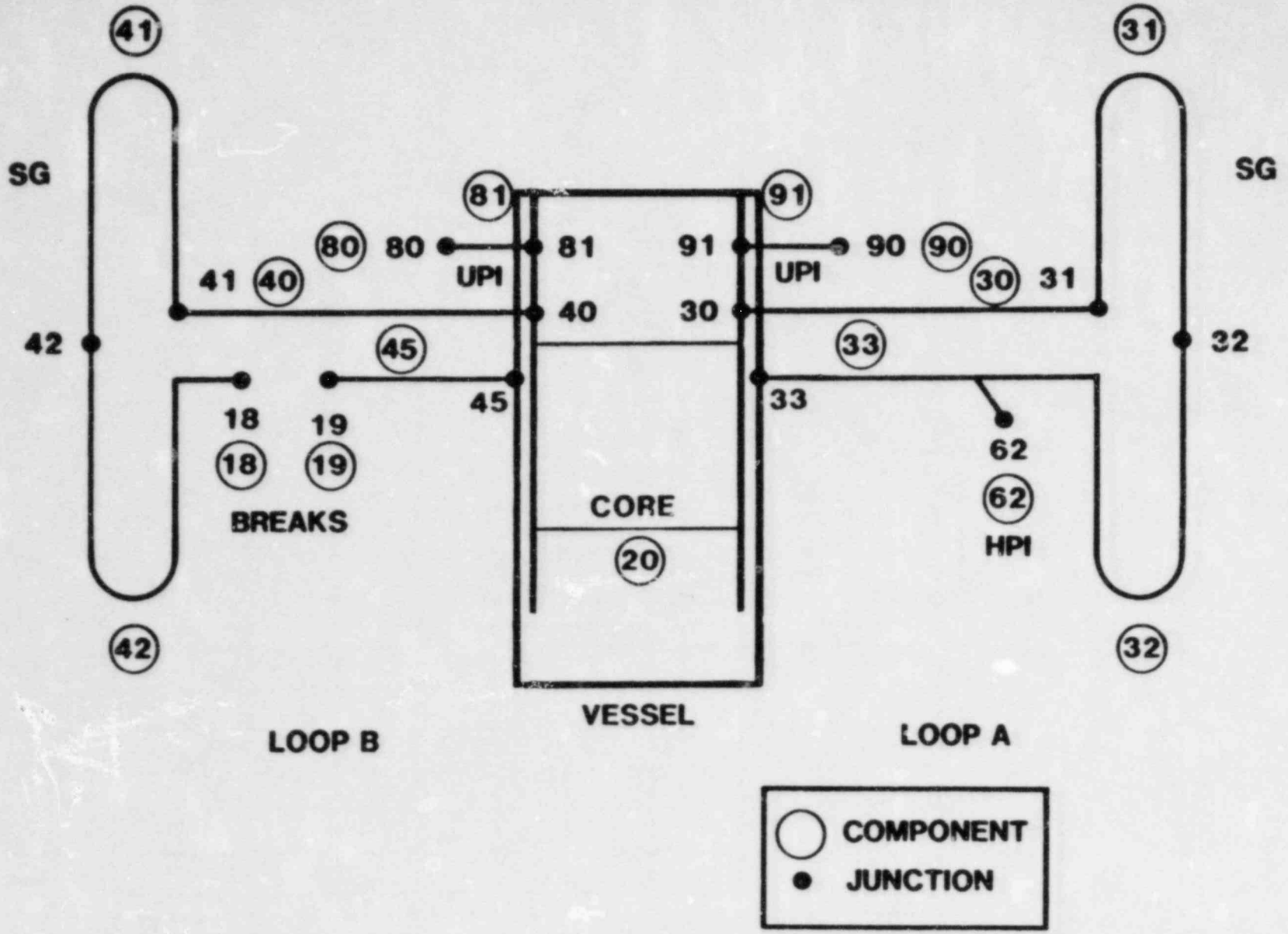

Figure 32. Westinghouse two-loop PWR TRAC schematic, detailed model.

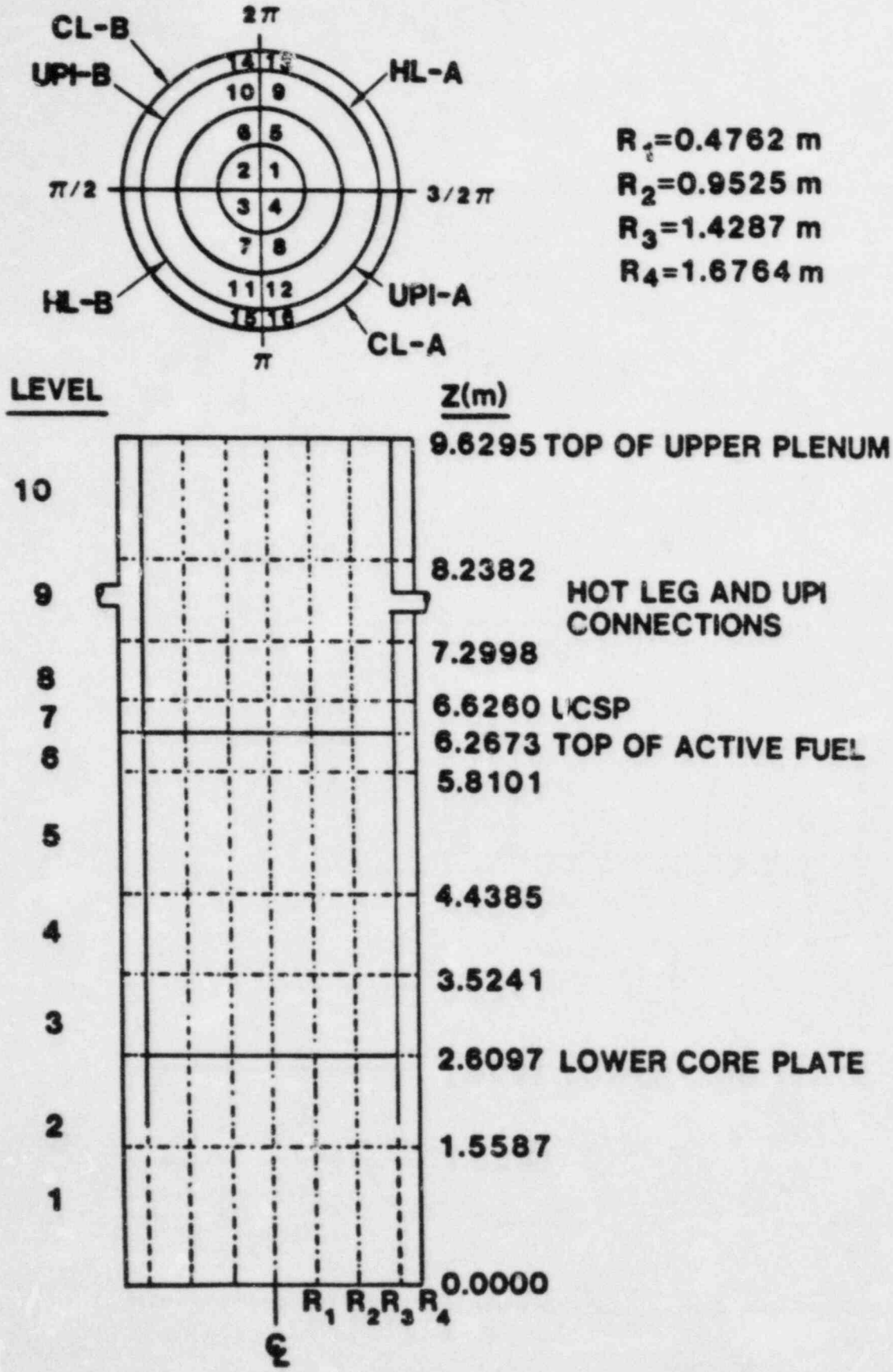

Figure 33. Vessel noding diagram, detailed model.

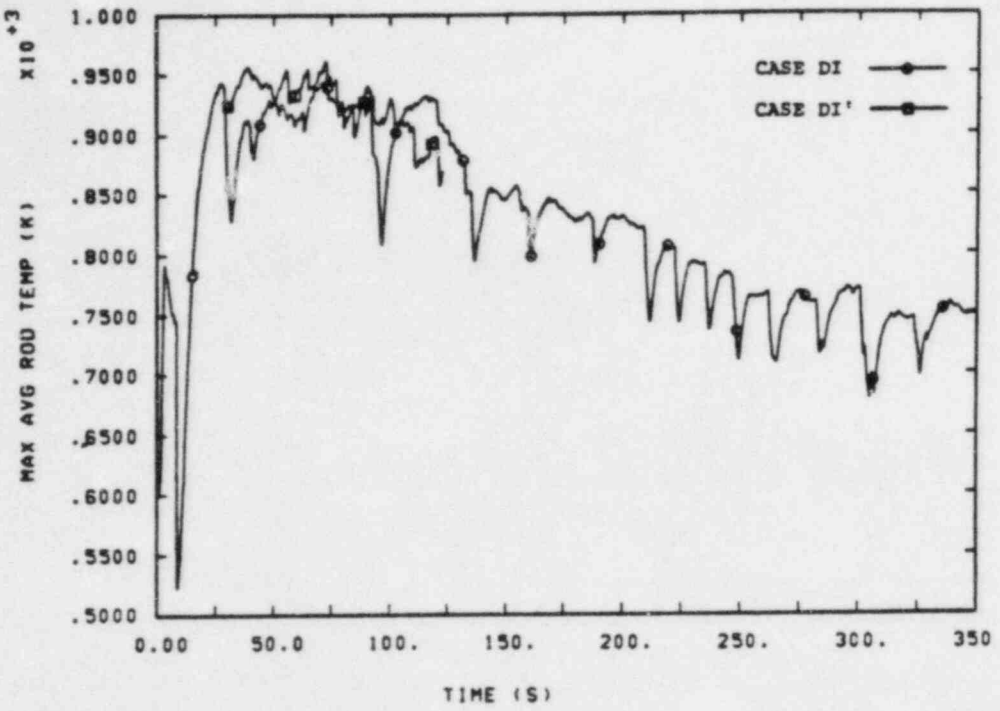

Figure 34. Maximum average-rod clad temperature. Case DI' predicts slightly higher PCT than Case DI.

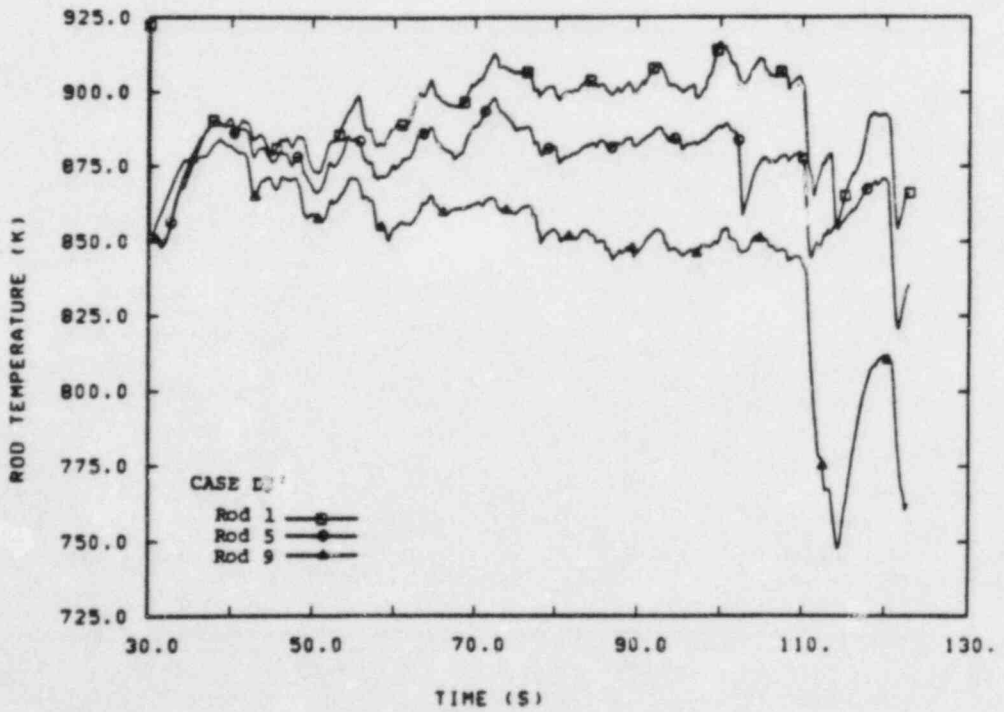

Figure 35. Clad temperatures at 2.2803 m core elevation, rods 1, 5, and 9. The radial power distribution is reflected by the radial temperature variations.

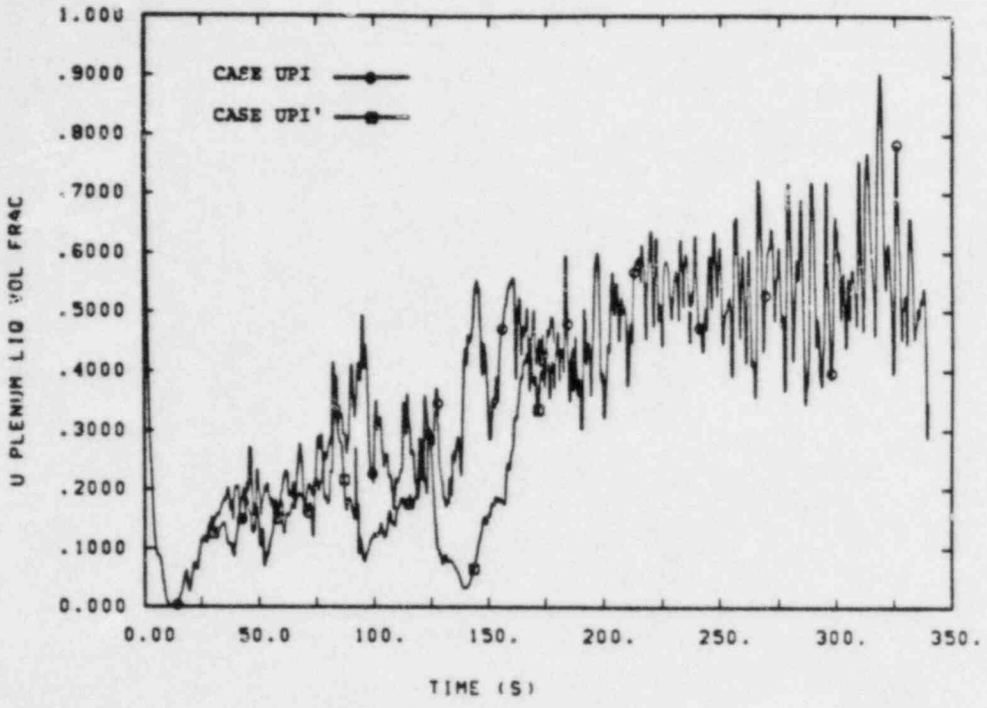

Figure 36. Upper plenum liquid volume fraction. Detailed model predicts slightly smaller pool formation on UCSP.

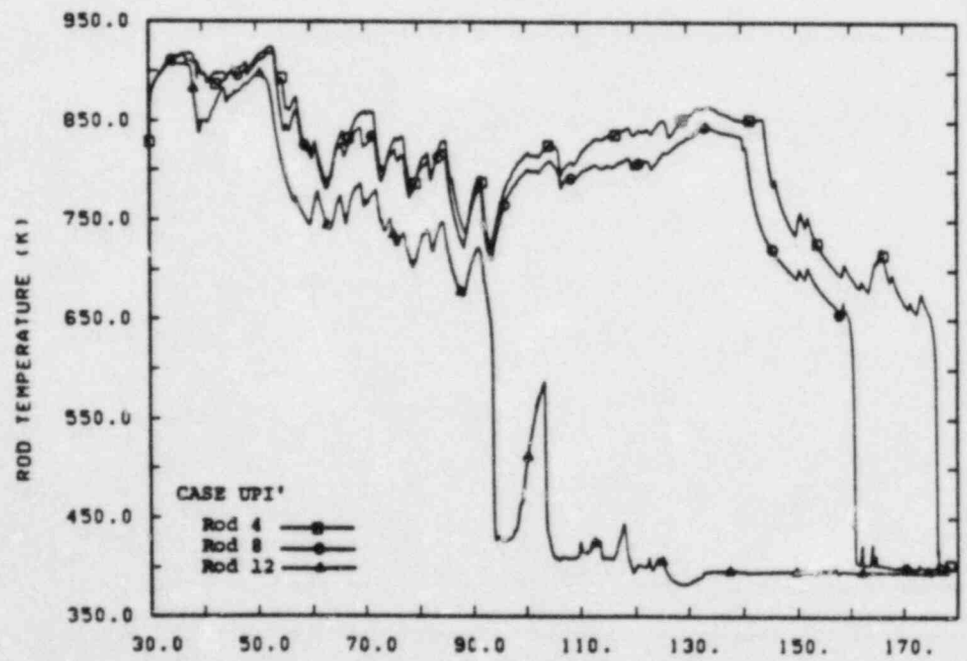

Figure 37. Clad temperatures at 1.3703 m core elevation, rods 4, 8, and 12. Early quenching of outer rods demonstrates effects of channeling.

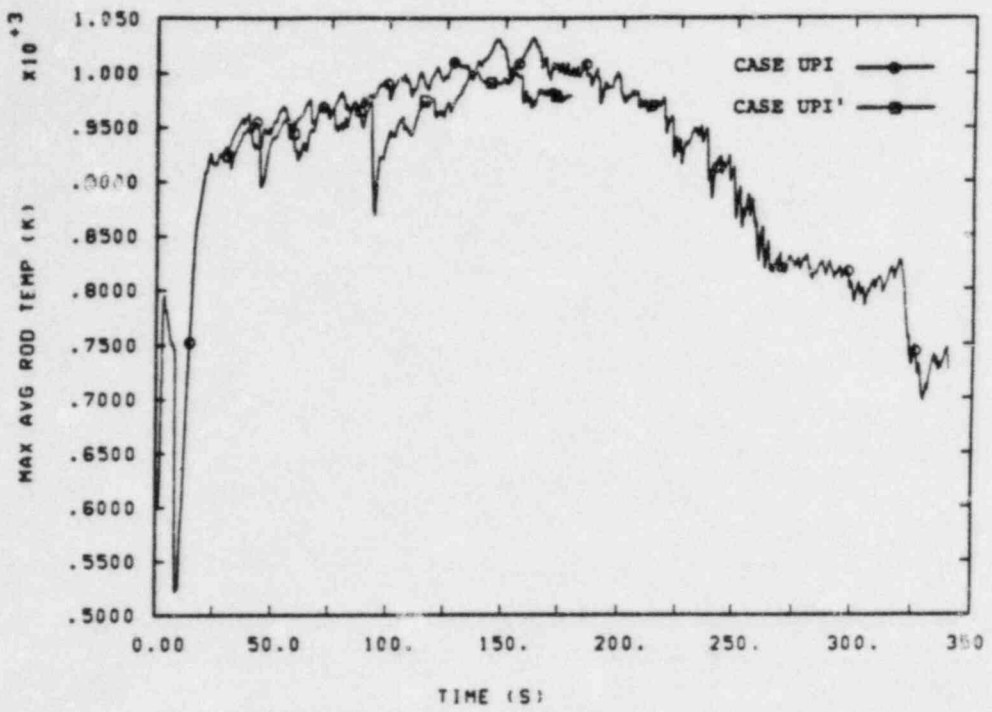

Figure 38. Maximum average-rod clad temperature. A lower PCT for Case UPI' is a result of LPI channeling.

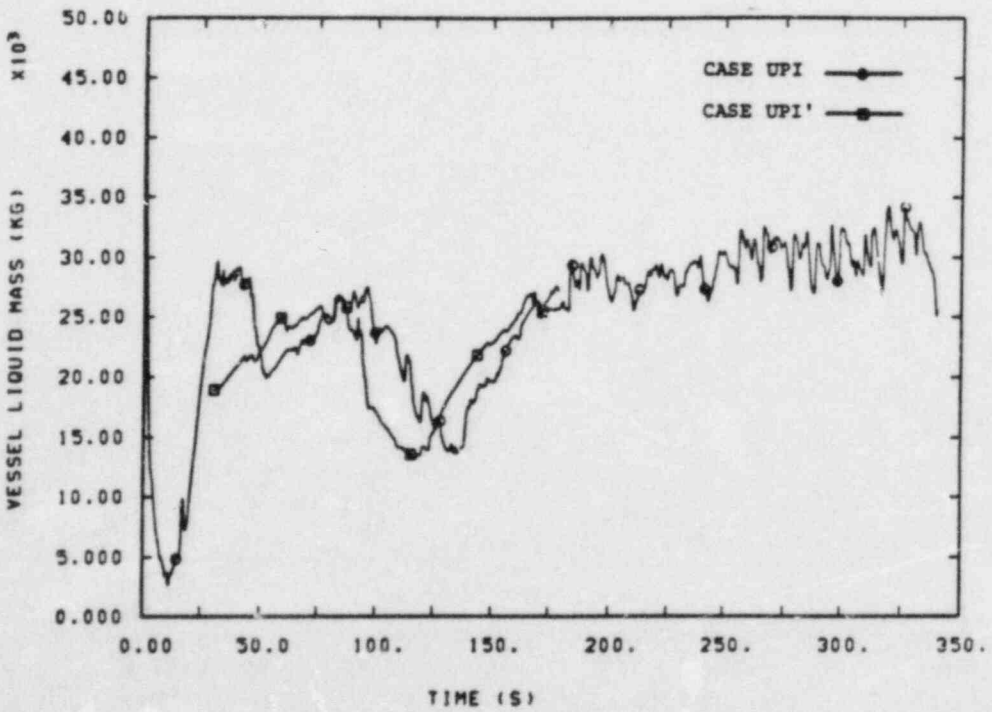

Figure 39. Vessel liquid mass. Vessel inventories for Case UPI' and Case UPI are very similar.

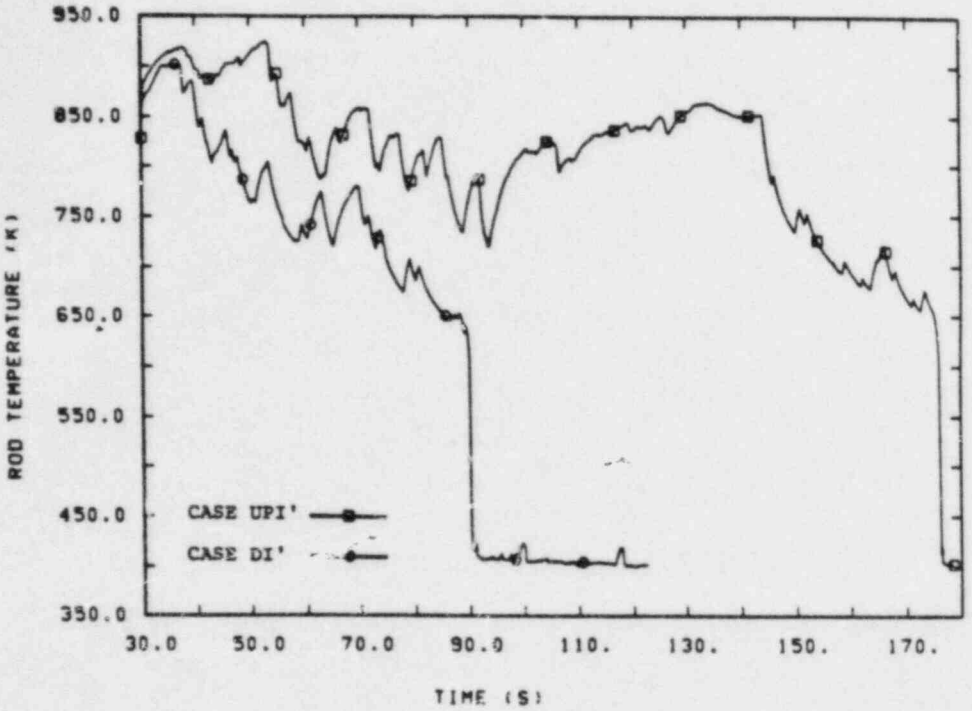

Figure 40. Clad temperature at 1.3703 m core elevation, rod 4. Downcomer injection results in better bottom reflood than upper plenum injection.

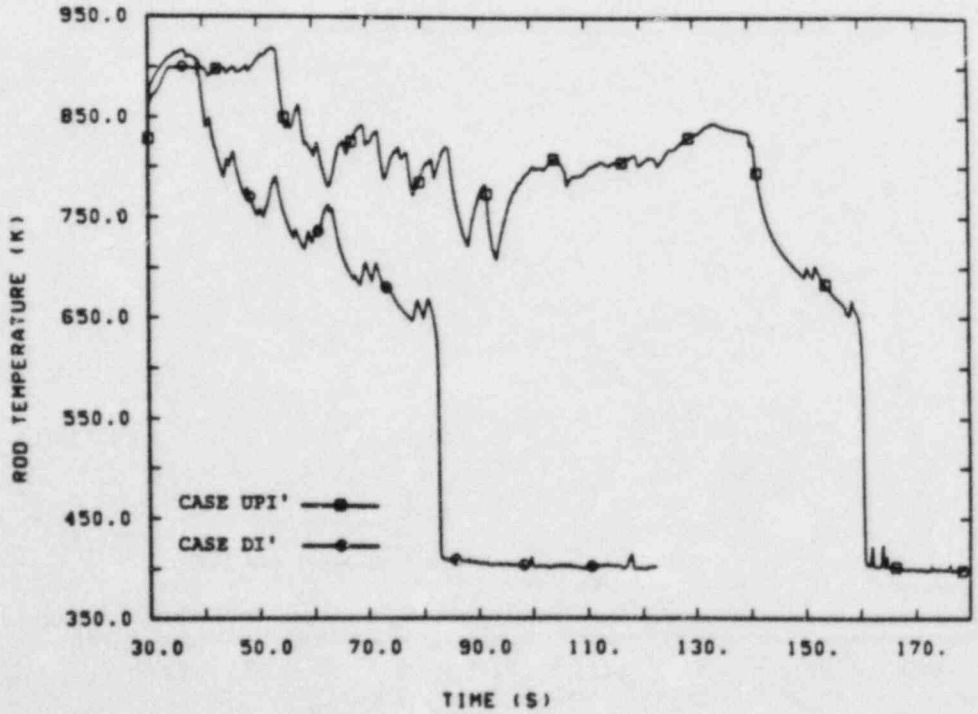

Figure 41. Clad temperature at 1.3703 m core elevation, rod 8.

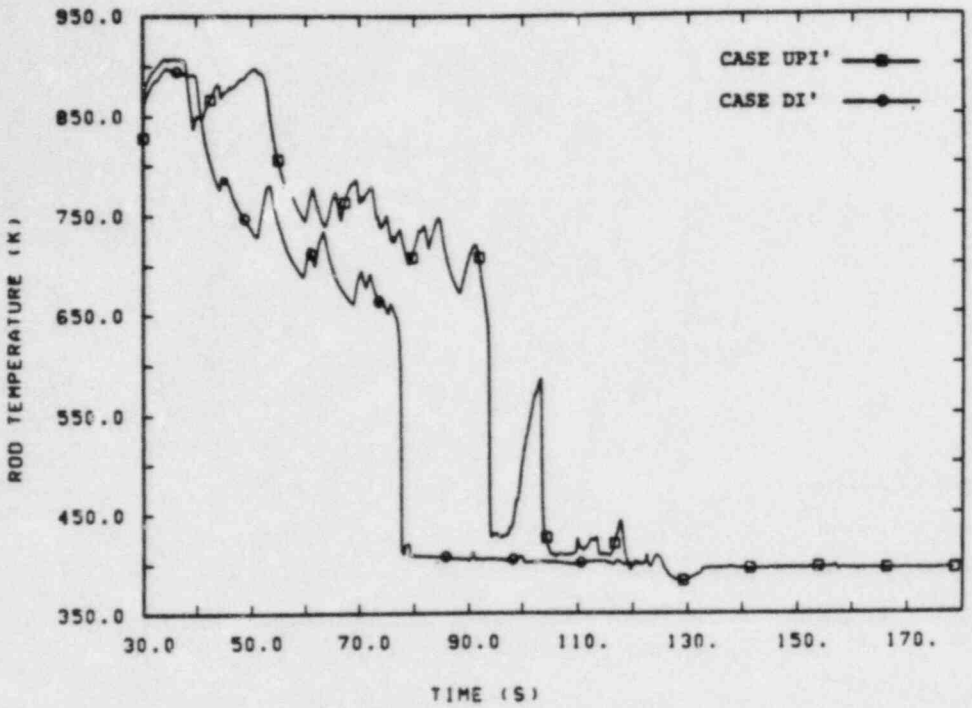

Figure 42. Clad temperature at 1.3703 m core elevation, rod 12.

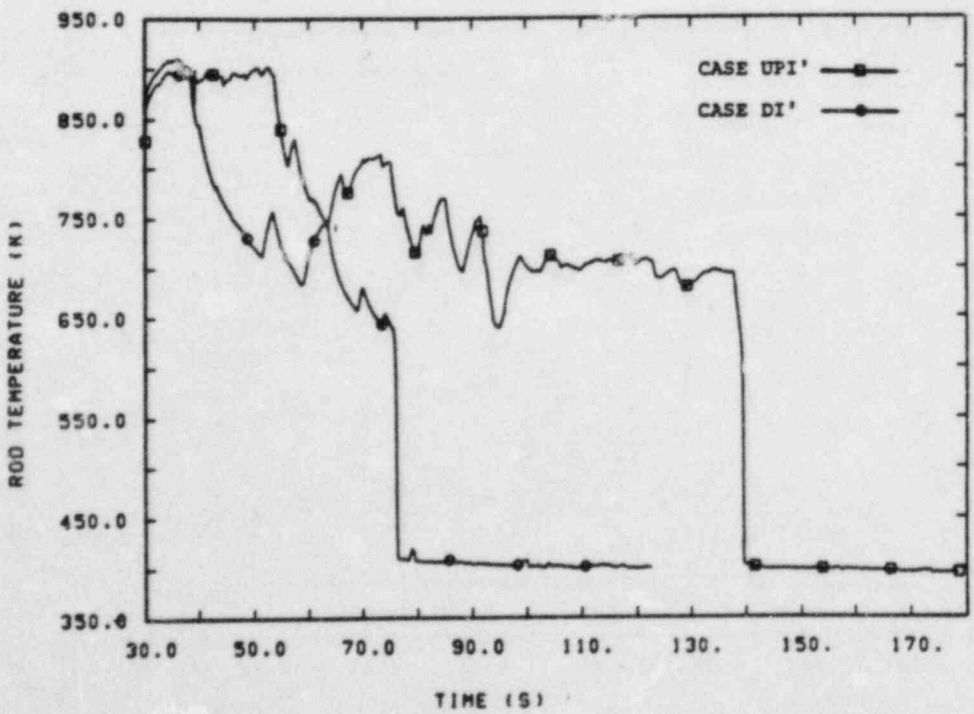

Figure 43. Clad temperature at 1.3703 m core elevation, rod 9.

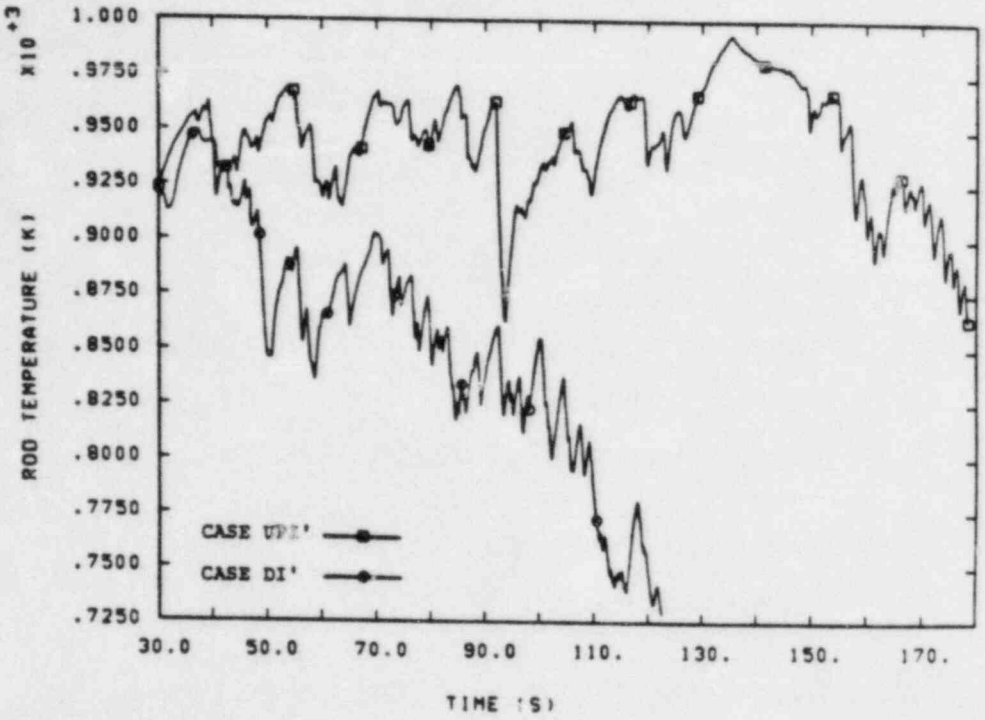

Figure 44. Clad temperature at 1.8288 m core elevation, rod 4, (midplane).

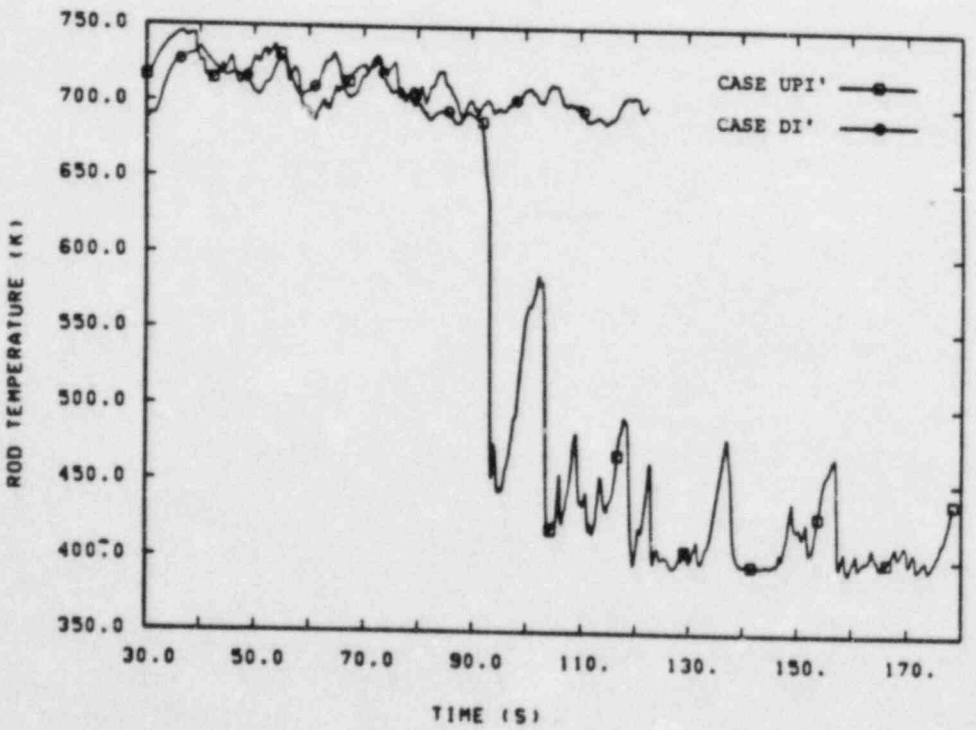

Figure 45. Clad temperature at 3.2003 m core elevation, rod 1. Upper plenum injection results in falling-film quench front.

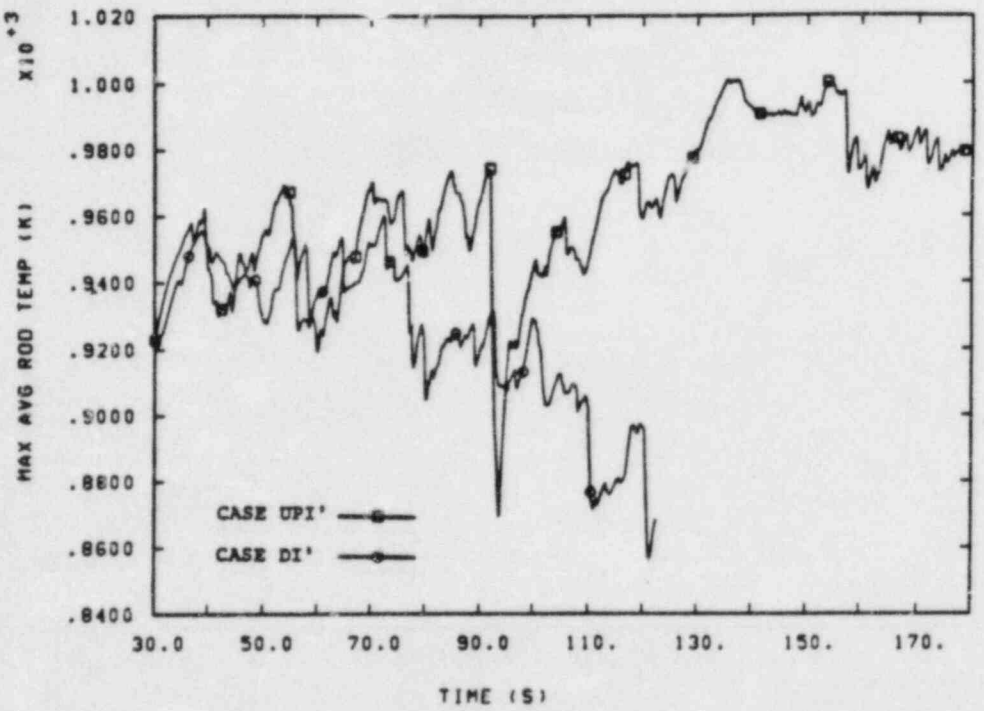

Figure 46. Maximum average-rod clad temperature. Upper plenum injection not as effective as downcomer injection.

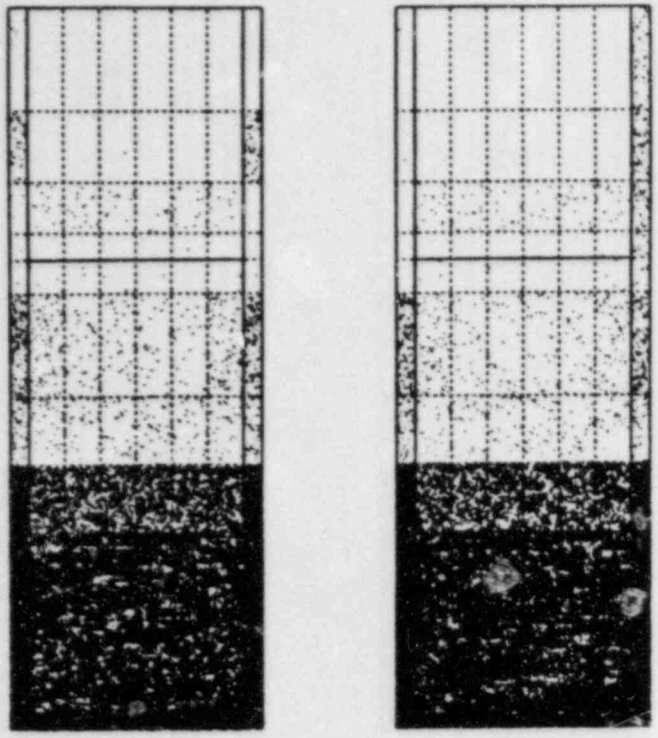

Figure 47. Liquid distribution, Case DI', time = 30 s.

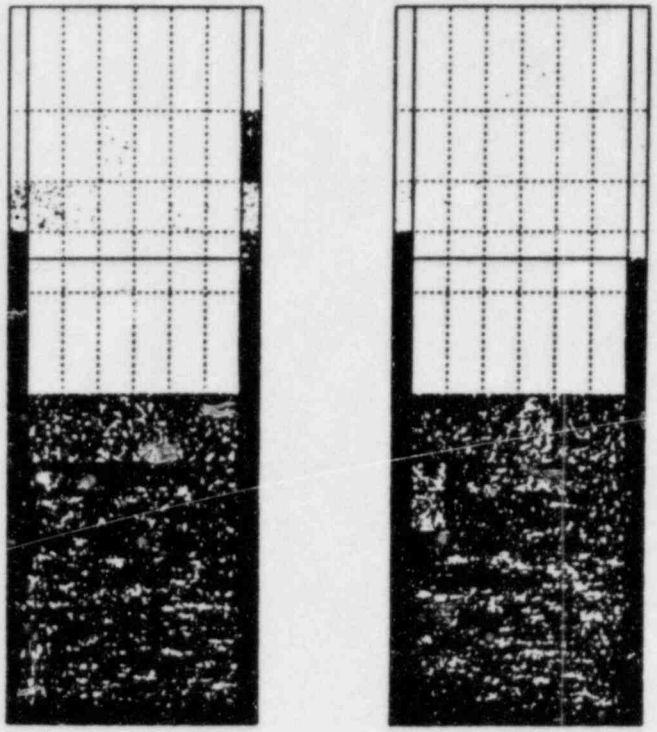

Figure 48. Liquid distribution, Case DI', time = 55 s.

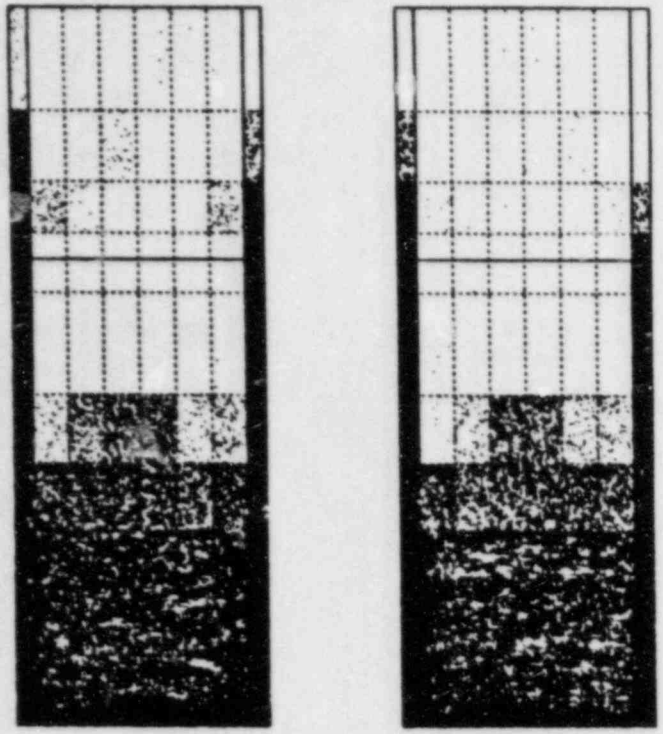

Figure 49. Liquid distribution, Case DI', time = 60 s.

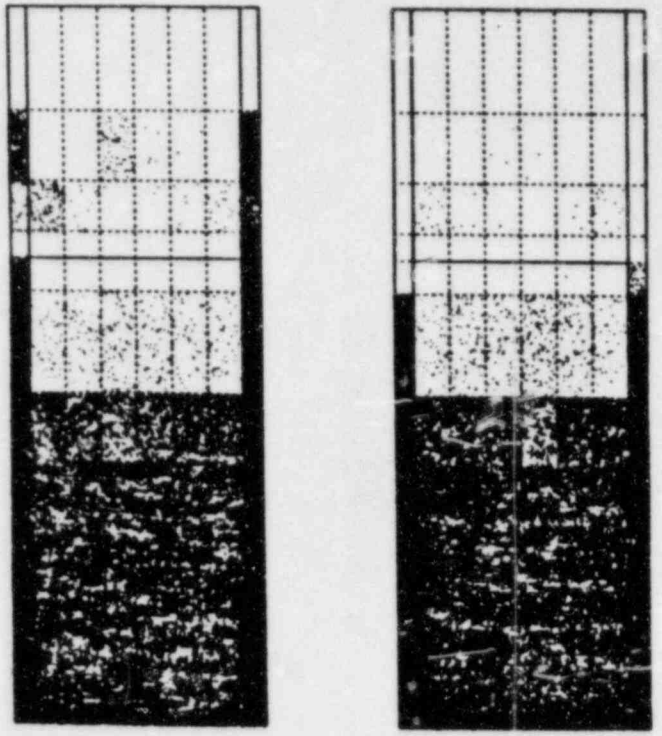

Figure 50. Liquid distribution, Case DI', time = 65 s.

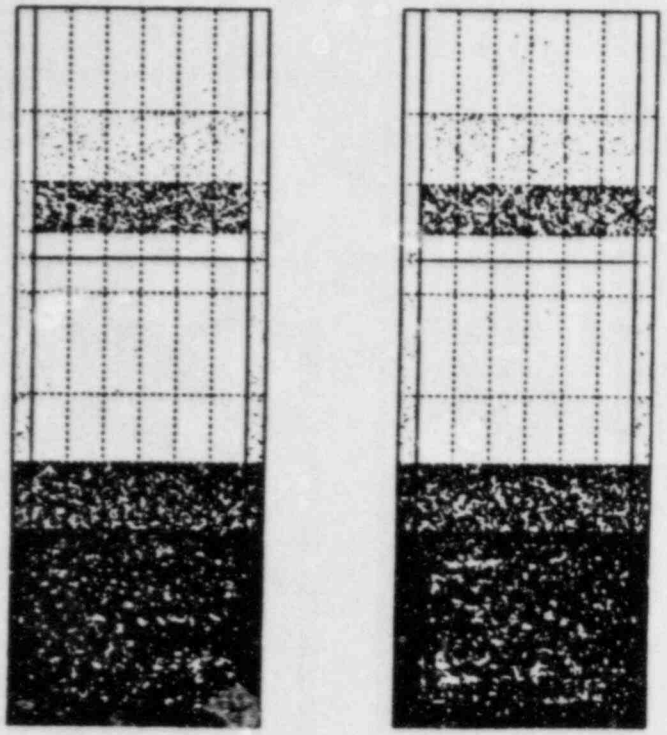

Figure 51. Liquid distribution, Case UPI', time = 30 s.

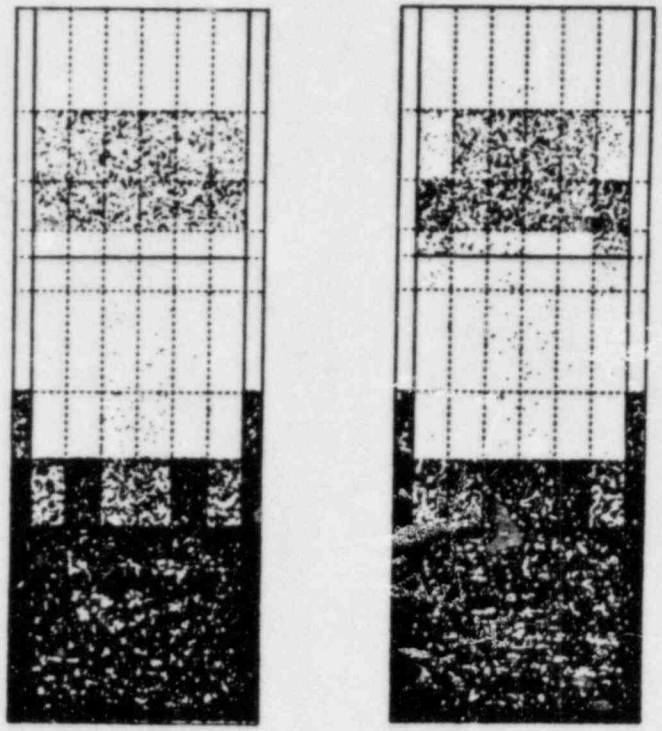

Figure 52. Liquid distribution, Case UPI', time = 34 s.

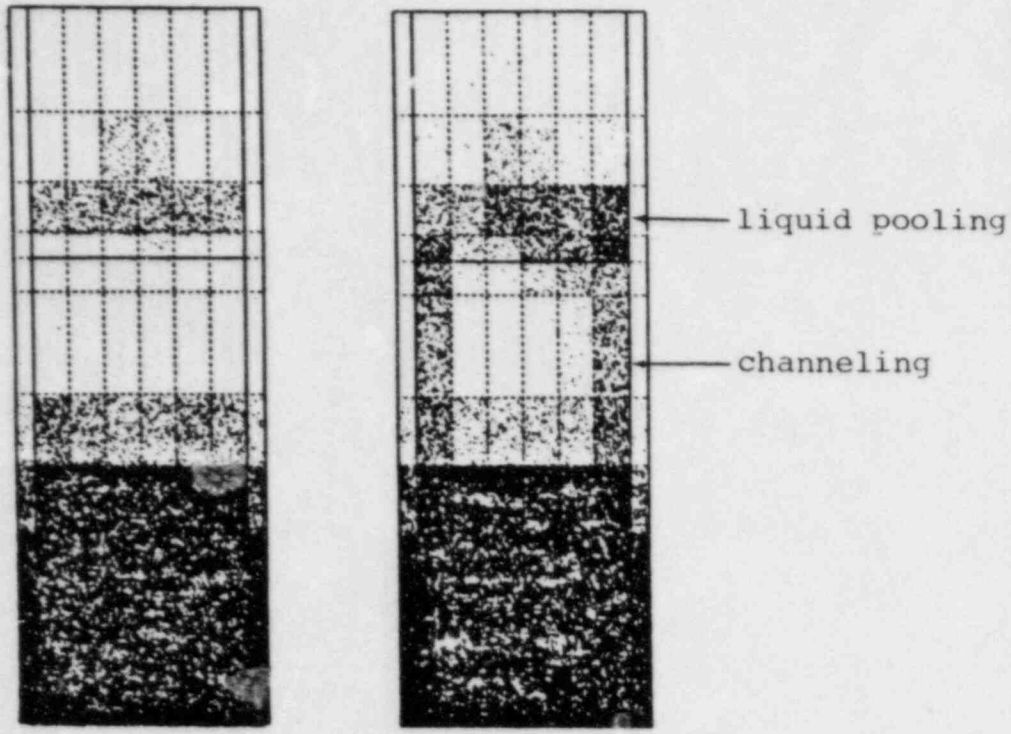

Figure 53. Liquid distribution, Case UPI', time = 38 s.

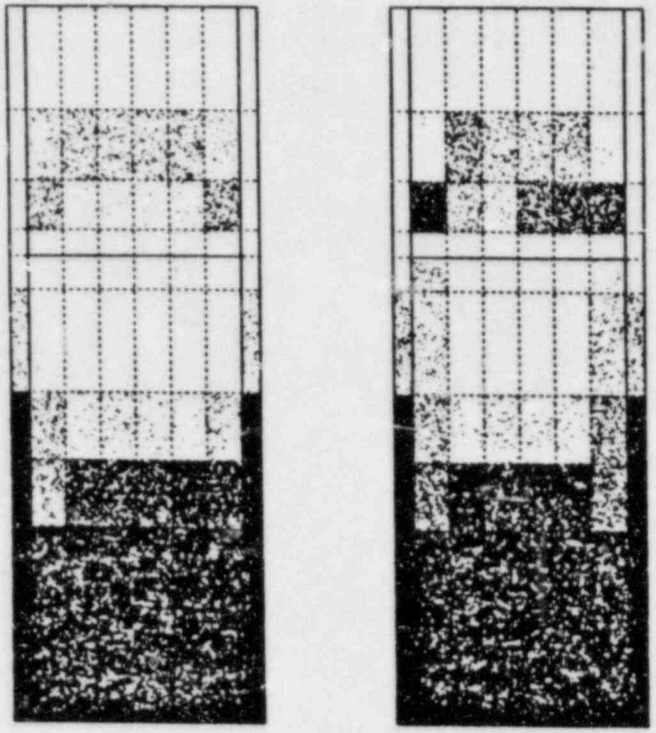

Figure 54. Liquid distribution, Case UPI', time = 40 s.

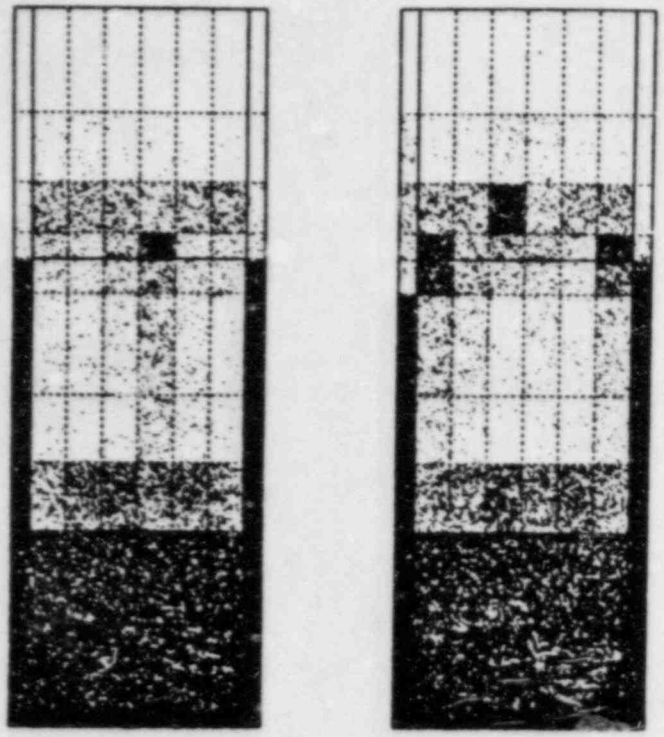

Figure 55. Liquid distribution, Case UPI', time = 50 s.

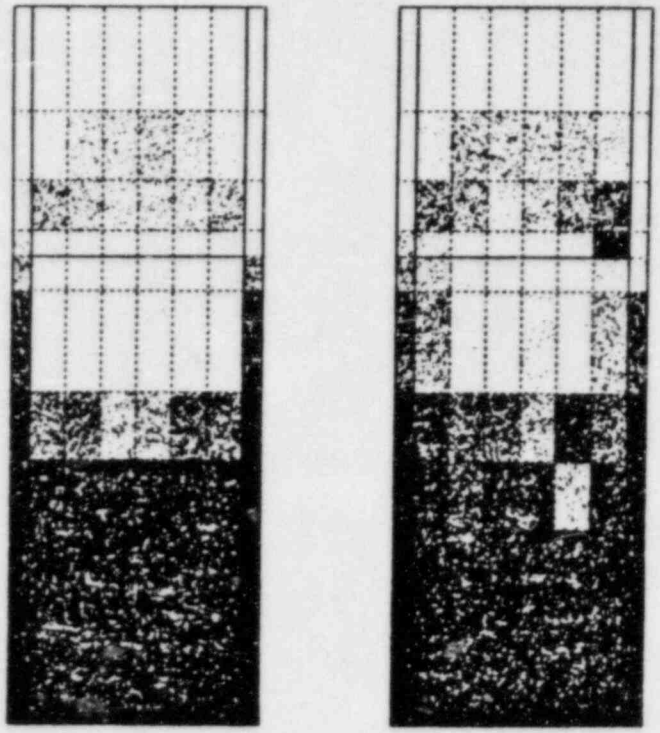

Figure 56. Liquid distribution, Case UPI', time = 55 s.

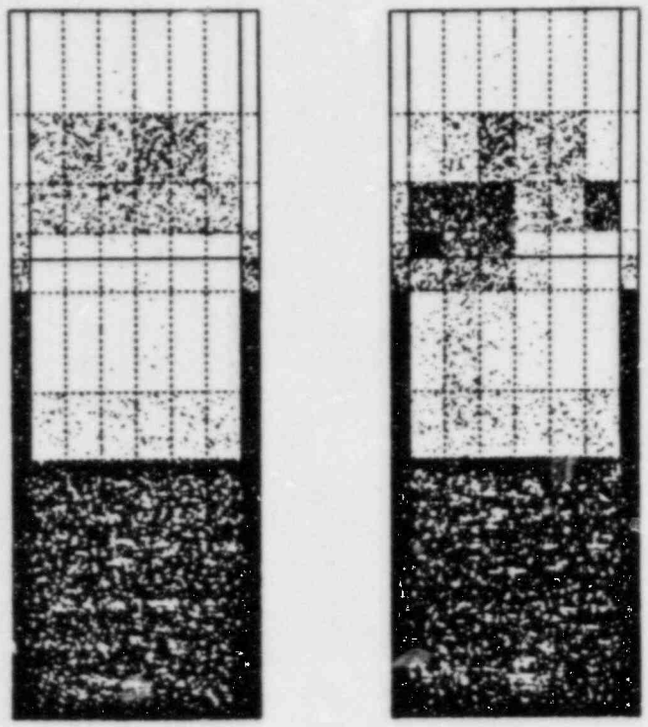

Figure 57. Liquid distribution, Case UPI', time = 65 s.

APPENDIX A: CALCULATION TIMING STATISTICS

Table A.I: Timing Statistics - Part 1

Case	CRAY-1 cpu(s)	Transient Time(s)	Number of Steps	Average Timestep Size(ms)
UPI	61,200	330	57,592	5.73
DI	46,800	350	44,381	7.88
UPI'	61,200	145	19,815	7.32
DI'	48,600	100	14,288	7.00

Table A.II: Timing Statistics - Part 2

Case	cpu/s	cpu/s/cell	cpu/step(s)	cpu/step/cell(ms)
UPI	185	1.022	1.063	5.871
DI	134	0.740	1.055	5.826
UPI'	422	2.209	3.089	16.17
DI'	486	2.545	3.401	17.81

APPENDIX B: FLOODING CALCULATIONS

$$j_g^{*1/2} + Mj_f^{*1/2} = C \qquad \text{Wallis Flooding Correlation}$$

where:
$$j_g^* = \frac{G_g}{gD_H\rho_g\,(\rho_f - \rho_g)^{1/2}}$$

$$j_f^* = \frac{G_f}{gD_H\rho_f\,(\rho_f - \rho_g)^{1/2}}$$

Let M = 1 and C = .8

For complete Flooding:

$$j_g^* = C^2$$

$$G_g = m_g/A$$

so
$$m_g = AC^2\,gD_H\rho_g\,(\rho_f - \rho_g)^{1/2}$$

where m_g is the vapor mass flow required for complete flooding

$\rho_g = 1.5\ kg/m^3$ $\quad \rho_f = 900\ kg/m^3$

$D_h = .0136m$ $\quad A = 2.5\ m^2$ $\quad g = 9.8\ m^2/s$

$$\therefore\ m_g = 21.4\ kg/s$$

(If C = 1.0, then m_g = 33.5 kg/s)

DISTRIBUTION: LARGE BREAK LOCA ANALYSES FOR TWO-LOOP PWRs
WITH UPPER PLENUM INJECTION
SAND84-0040

U. S. NRC Distribution Contractor (CDSI)
7300 Pearl Street
Bethesda, MD 20014

U. S. Nuclear Regulatory Commission
Reactor Systems Branch
Division of Systems Integration
Office of Nuclear Reactor Regulation
Washington, DC 20555
Attn: Brian W. Sheron, P-1132
David Langford, P-1132
G. Norman Lauben, P-1132

U. S. Nuclear Regulatory Commission
Operating Reactors Branch #1
Division of Licensing
Office of Nuclear Regulatory Research
Washington, DC 20555
Attn: Marshall Grotenhuis, MS-438

Exxon Nuclear Company, Inc.
Reload Fuel Licensing
2101 Horn Rapids Road
P. O. Box 130
Richland, Washington 99352
Attn: John C. Chandler
Robert A. Copeland

Westinghouse Electric Corporation
P. O. Box 355
Pittsburgh, PA 15230
Attn: R. M. Kemper
L. E. Hochreiter

Professor F. Mayinger
Lehrstuhl A fur Thermodynamik
Archisstrasse 21
8000 Munchen 2
Munich, West Germany

Dr. K. Hirano
Japan Atomic Energy Research Inst.
Tokai-Mura, Naka-Gun
Ibaraki-Ken, Japan

Dr. N. Zuber
U. S. Nuclear Regulatory Commission
Reactor Systems Research Branch
Washington, D. C. 20555
(Mail Stop 1130-SS)

Dr. Y. Murao
Japan Atomic Energy Research Inst.
Tokai-Mura, Naka-Gun
Ibaraki-Ken, Japan

Dr. K. Hofmann
Gesellschaft Fur Reactorsicherheit
2, Glockengasse
5 Koln 1
Federal Republic of Germany

Dr. F. Winkler
Kraftwerk Union
Aktiengesellschaft
Hammerbacherstrasse 12 + 14
Postfach 32 20
D-8520 Erlangen
Federal Republic of Germany

Dr. M. Sawitzki
Kraftwerk Union
Aktiengesellschaft
Hammerbacherstrasse 12 + 14
Postfach 32 20
D-8520 Erlangen
Federal Republic of Germany

Dr. L. Shotkin
U. S. Nuclear Regulatory Commission
Reactor Systems Research Branch
Washington, D. C. 20555
(Mail Stop 1130-SS)

Dr. G. Rhee
U. S. Nuclear Regulatory Commission
Reactor Systems Research Branch
Washington, D. C. 20555
(Mail Stop 1130-SS)

Dr. Y. S. Chen
U. S. Nuclear Regulatory Commission
Reactor Systems Research Branch
Washington, D. C. 20555
(Mail Stop 1130-SS)

Dr. K. Williams
Los Alamos National Laboratory
P. O. Box 1663
Los Alamos, New Mexico 87545

Dr. D. Chapin
MPR Associates, Incorporated
1050 Connecticut Avenue, N.W.
4th Floor
Washington, D. C. 20036

Mr. J. Colson
EG&G Idaho, Incorporated
550 Second Street
Idaho Falls, Idaho 83401
(Location: TSB)

Mr. M. Herskovitz
Oak Ridge National Laboratory
Post Office Box Y
Oak Ridge, Tennessee 37830
(Mail Stop 006)

6400 A. W. Snyder
6410 J. W. Hickman
6417 D. C. Carlson
6420 J. V. Walker
6421 T. R. Schmidt
6422 D. A. Powers
6423 P. S. Pickard
6425 W. J. Camp
6427 M. Berman
6427 C. C. Wong
6440 D. A. Dahlgren
6442 W. A. von Riesemann
6444 S. L. Thompson (2)
6444 L. D. Buxton (10)
6444 R. K. Byers
6444 R. K. Cole, Jr.
6444 P. N. Demmie
6444 D. Dobranich (5)
6444 M. G. Elrick
6444 L. N. Kmetyk
6444 R. Knight
6444 J. M. McGlaun
6444 J. Orman
6444 A. C. Peterson
6444 W. R. Schmidt
6444 R. M. Summers
6444 S. W. Webb
6444 G. G. Weigand
6449 K. D. Bergeron
3141 C. M. Ostrander (5)
3151 W. L. Garner
8424 M. A. Pound

NRC FORM 335 (6-83) U.S. NUCLEAR REGULATORY COMMISSION

BIBLIOGRAPHIC DATA SHEET

1 REPORT NUMBER (Assigned by TIDC, add Vol. No., if any)
NUREG/CR-3639
SAND84-0040

2 Leave blank

3 TITLE AND SUBTITLE
LARGE BREAK LOCA ANALYSES FOR TWO-LOOP PWRs WITH UPPER-PLENUM INJECTION

4 RECIPIENT'S ACCESSION NUMBER

5 DATE REPORT COMPLETED
MONTH: February YEAR: 1984

6 AUTHOR(S)
D. Dobranich, L.D. Buxton

7 DATE REPORT ISSUED
MONTH: May YEAR: 1984

8 PERFORMING ORGANIZATION NAME AND MAILING ADDRESS (Include Zip Code)
Sandia National Laboratories
Albuquerque, NM 87185

9 PROJECT/TASK/WORK UNIT NUMBER

10 FIN NUMBER
A-1294

11 SPONSORING ORGANIZATION NAME AND MAILING ADDRESS (Include Zip Code)
Division of Systems Integration
Office of Nuclear Reactor Regulation
U. S. Nuclear Regulatory Commission
Washington, DC 20555

12a TYPE OF REPORT
Technical

12b PERIOD COVERED (Inclusive dates)

13 SUPPLEMENTARY NOTES

14 ABSTRACT (200 words or less)

A series of best-estimate thermal-hydraulic calculations was performed using TRAC-PF1 to simulate a hypothetical loss-of-coolant accident in Westinghouse two-loop pressurized water reactors. Those reactors are equipped for low-pressure injection of emergency coolant directly into the upper plenum of the reactor vessel. This type of injection is referred to as upper plenum injection (UPI). The calculations were performed to evaluate the effectiveness of UPI compared to injection into the vessel downcomer, referred to as downcomer injection (DI).

The TRAC results indicated that some channeling of upper plenum injected liquid down the core periphery occurred; however, a large percentage of that liquid was vaporized as it drained toward the lower plenum. This vaporization degraded the bottom-flood quench front compared to that seen in TRAC calculations in which downcomer injection was assumed. For the case of upper plenum injection, counter-current flow limiting conditions at the upper core support plate led to formation of a large subcooled liquid pool in the upper plenum; part of this subcooled liquid was entrained into the hot legs and steam generators. Only a small saturated liquid pool formed in the case of downcomer injection. Overall, the calculations show that higher peak clad temperatures are produced when the low-pressure injection is into the upper plenum instead of the vessel downcomer.

15a KEY WORDS AND DOCUMENT ANALYSIS

15b DESCRIPTORS
TRAC - PF 1 (Transient Reactor Analyses Code)
LOCA
PCT
Cold Leg

16 AVAILABILITY STATEMENT
Unlimited

17 SECURITY CLASSIFICATION (This report)
Unclassified

18 NUMBER OF PAGES

19 SECURITY CLASSIFICATION (This page)

20 PRICE
$

UNITED STATES
NUCLEAR REGULATORY COMMISSION
WASHINGTON, D.C. 20555